Sensitivity of precipitation and temperature over Mount Kenya area to physics parameterization options in a high-resolution model simulation performed with WRFV3.8.1

Martina Messmer[1,2,3], Santos J. González-Rojí[1,2], Christoph C. Raible[1,2], and Thomas F. Stocker[1,2]

[1]Climate and Environmental Physics, University of Bern, Bern, Switzerland
[2]Oeschger Centre for Climate Change Research, University of Bern, Bern, Switzerland
[3]School of Earth Sciences, The University of Melbourne, Melbourne, Victoria, Australia

Correspondence: Martina Messmer (martina.messmer@climate.unibe.ch)

Abstract. Several sensitivity experiments with the Weather Research and Forecasting (WRF) model version 3.8.1 have been performed to find the optimal parameterization setup for precipitation amounts and patterns around Mount Kenya at a convection-permitting scale of 1 km. Hereby, the focus is on the cumulus scheme, with tests of the Kain-Fritsch, the Grell-Freitas and no cumulus parameterization. Besides, two long wave radiation schemes and two planetary boundary layer parameterizations are evaluated. Additionally, different nesting ratios and numbers of nests are tested. The precipitation amounts and patterns are compared against a large number of weather station data and three gridded observational data sets. The temporal correlation of monthly precipitation sums show that fewer nests lead to a more constrained simulation and hence, the correlation is higher. The pattern correlation with weather station data confirms this result, but when comparing it to the most recent gridded observational data set the difference between the number of nests and nesting ratios are marginal. The precipitation patterns further reveal that using the Grell-Freitas cumulus parameterization in the domains with resolutions > 5 km provides the best results, when it comes to precipitation patterns and amounts. If no cumulus parameterization is used in any of the domains, the temporal correlation between gridded and in-situ observations and simulated precipitation is especially poor with more nests. Moreover, even if the patterns are captured reasonably well, a clear overestimation in the precipitation amounts is simulated around Mount Kenya when using no cumulus scheme in all domains. The experiment with the Grell-Freitas cumulus parameterization in the domains with resolutions > 5 km also provides reasonable results for 2-metre temperature with respect to gridded observational and weather station data.

1 Introduction

East Africa, including Kenya, has anomalously dry climate conditions compared to many other equatorial regions around the globe (e.g., Trewartha, 1981; Nicholson, 2017). The precipitation patterns in East Africa are very heterogeneous, which can

be attributed to the variety and complexity of large-scale controls, i.e., topography, influence from the ocean, the dynamics of the tropical circulation and lakes (Nicholson, 2017). The topography, in particular the Turkana channel between the Ethiopian and East African highlands in Kenya, exerts a strong steering effect on the low-level flow on time scales from seasons to days (Paegle and Geisler, 1986; Slingo et al., 2005). The Turkana jet has an influence on the local climate and especially on precipitation, and a study by Nicholson (2016a) suggests that it might even be responsible for the suppression of the summer rainy season in northwestern Kenya. The zonal circulation over the Indian Ocean further influences precipitation in Kenya, as it is located under subsiding air masses, leading to the aforementioned aridity over an equatorial region (Pohl and Camberlin, 2011; Nicholson, 2017). Weak equatorial zonal circulations are typically associated with floods at the coasts of East Africa, which coincide with scarce rain over Indonesia (Hastenrath and Polzin, 2004, 2005). This circulation and thus, the intensity and the vertical extent of the subsidence account for variations in the inter-annual rainfall variability over Kenya (Pohl and Camberlin, 2011; Nicholson, 2017). The second largest freshwater lake in the world, Lake Victoria, also contributes to rainfall in this area. It generates its own mesoscale atmospheric circulation system that leads to high rainfall amounts over the lake, where lake surface temperatures are strongly related to the rainfall amounts (Sun et al., 2014). Furthermore, local thunderstorms with heavy precipitation can be triggered over Lake Victoria, rendering the lake-land breeze but also large-scale moisture availability as the main control (Thiery et al., 2015; Woodhams et al., 2019).

All these large-scale controls lead to the fact that the climate in Kenya is characterized by two rainy seasons. The March-April-May (MAM) season is often termed as 'long rains', as this season is associated with the longest lasting and heaviest precipitation events, which in some years can even end up in floods (e.g., Kilavi et al., 2018). The other rainy season is called 'short rains' and occurs in October-November (ON). It plays a less important role in the total amount of precipitation, but accounts for most of the inter-annual variability (Camberlin and Philippon, 2002; Hastenrath et al., 2010). Thus, it is not surprising that the 'short rains' are responsible for both floodings and droughts. The occurrence of floods in Kenya is not unusual, and often floods set in after very dry years (Parry et al., 2012; Kilavi et al., 2018). Droughts are found to be related to El Niño–Southern Oscillation (ENSO) events on inter-annual timescales (Nicholson, 2015), as it affects the atmospheric circulation over the Indian Ocean and the strength and formation processes of the Indian Ocean dipole (Behera et al., 2006). This circulation has also an impact on the 'short rains' in East Africa (Pohl and Camberlin, 2011; Nicholson, 2016b). In general, moisture convergence and increased convective activity over East Africa are associated with positive SST anomalies over the western equatorial Indian Ocean (Saji et al., 1999; Ummenhofer et al., 2009). Additionally, the Madden-Julian-Oscillation can impact precipitation on inter-seasonal timescales and it is able to strengthen or weaken the climatological convective and dynamic zonal gradients between Southeast Asia and East Africa (Pohl and Camberlin, 2011). The low-level jet stream in the Turkana channel is also suggested to be able to enhance extremes in precipitation over East Africa (Nicholson, 2016b). Nevertheless, in the recent past, droughts instead of floods are of major concern in Kenya. The more frequent occurrence of droughts seems to be related to a negative trend in the 'long rains' in MAM starting in the 1980s and lasted up to the late 2000s (Williams and Funk, 2011; Liebmann et al., 2014; Ayugi et al., 2016). Wainwright et al. (2019) suggested that this negative trend is caused by a shortening of the rainy season rather than a decline in daily precipitation, as the tropical rain-band moves faster to the north during the 'long rains'.

The rather sparse observation network in East Africa and also Kenya in combination with the aforementioned complexity of the climate, conspire against obtaining a better understanding of all the involved processes that dominate the climate, but also its changes. To overcome this issue, climate models, and in particular regional climate models, could help understanding those processes in more detail. Nevertheless, capturing the convective precipitation in the tropics correctly is also a challenge for regional climate models, and that is why several studies focus on the evaluation of their performance in different regions (e.g., Rauscher et al., 2010; Kendon et al., 2017; Brune et al., 2020; Wu et al., 2020).

Only in the past few years the number of climate simulations over Africa or over Eastern Africa has increased. At the same time, the resolution of these simulations has become much finer. Cook and Vizy (2013) performed a simulation over entire Africa using the Weather Research and Forecasting (WRF) Model (Skamarock et al., 2008) at a 90 km horizontal resolution. They concluded that the model is able to capture the distribution of the precipitation and the corresponding circulation quite well over Eastern Africa, but a wet bias in the model simulation remains. Williams et al. (2015) found an overestimation of precipitation and a well captured spatial pattern over the Lake Victoria basin, which is inline with the results found in Cook and Vizy (2013). Williams et al. (2015) used the UK Met Office Hadley Centre Regional Climate Model at 50 km horizontal resolution over Africa. Two simulations, one with 50 and the other with 25 km resolution over Eastern Africa were also performed by Kerandi et al. (2017). They examined the representation of temperature and precipitation over the Tana river basin in Kenya, finding that temperature and precipitation patterns are well captured, but with a cold temperature bias. The increase in the resolution from 50 to 25 km resulted in a much better representation of precipitation (Kerandi et al., 2017). Otieno et al. (2019) performed different sensitivity studies with WRF to test the effect of four cumulus parameterizations (Kain-Fritsch, Kain–Fritsch with a moisture advection-based trigger function, Gréll-Dévényi, and Betts–Miller–Janjicon schemes) to the representation of precipitation over East Africa during wet years. The authors still used a rather coarse resolution of 36 km covering East Africa including parts of the Indian Ocean and the rain forest in Congo, i.e., two important moisture sources.

The most recent simulations over (Eastern) Africa access the convection-permitting scales (resolution finer than 5 km) (Stratton et al., 2018). This scale, and the ability to neglect the cumulus parameterization, can have a fundamental impact on model variables, in particular on precipitation (Ban et al., 2014; Giorgi et al., 2016; Gómez-Navarro et al., 2018). This is especially true for regions with high and complex topography such as East Africa. The simulation published in Stratton et al. (2018) is performed with the Met Office Unified Model at 4.5 km horizontal resolution. Due to its high spatial resolution, it is convection-permitting and hence, a cumulus parameterization is not needed. This simulation is investigated in more detail in Finney et al. (2019) with respect to East African climate and compared to a parameterized 25 km spatial resolution simulation. They found that especially the diurnal cycle in rainfall benefits from the convection-permitting resolution, but also precipitation intensities and patterns improve. Additionally, Woodhams et al. (2018) confirmed that a convection-permitting simulation is able to better represent the sub-daily precipitation intensities over Lake Victoria and the occurrence of storms over land. Another recent climate simulation at convection permitting scales using WRF (reaching 800 m in the innermost domain) was used to established the relationship between local atmospheric conditions over Kilimanjaro and El Niño–Southern Oscillation and the Indian Ocean zonal mode (Collier et al., 2018).

The studies presented above already indicate that there are several regional climate models (RCMs) available. Each of these models have different sets of parameterizations that can be chosen, and the ability to simulate the climate over a certain region depends to a large part on the selection of the different parameterization options. Several studies have evaluated the transferable skills of RCMs to different regions (e.g., Takle et al., 2007; Jacob et al., 2007; Rockel and Geyer, 2008; Jacob et al., 2012; Bellprat et al., 2016; Russo et al., 2019). A recent study (Russo et al., 2020) shows that the parameterization setting depends on the region of interest. Thus, there is a need to retune RCMs for different regions. Hence, this study presents a set of sensitivity studies performed by WRF, initiated and driven by ERA5, to find an optimal setting for the representation of precipitation in convection-permitting simulations over Mount Kenya.

In this paper, the focus on Mount Kenya is chosen, as it plays a crucial role in the supply of freshwater both in the highlands and in the surrounding lowlands (Liniger et al., 2005). The availability of fresh water decreases drastically with longer distances from Mount Kenya, and is further reduced by evapotranspiration from the vegetation in the drier savannas of the lowlands (Ngigi et al., 2007). Population growth through migration puts further pressure on water availability (Ngigi et al., 2007) which may result in disputes, marginalization and conflicts (Wiesmann et al., 2000). This situation is exacerbated by progressive climate change that will affect water availability through changes in precipitation amounts and patterns, induced by either local or large scale changes. To understand the behaviour of precipitation in this complex topographical area and to obtain possible adaptation strategies, it is vital to create reliable regional climate simulations that can also be used for climate projections in a next step.

The paper gives a detailed description of the sensitivity simulations performed with WRF, but also its initial and boundary conditions provided by the reanalysis data ERA5. Furthermore, the different observation based gridded data for precipitation and temperature and the weather station data are presented in Section 2. Section 3 provides an analysis of the temporal and spatial representation of precipitation patterns over the area around Mount Kenya. Also, the sensitivity of the different parameterization options to precipitation amounts and patterns are investigated. The analysis is topped off with a brief description of the 2-metre temperature around Mount Kenya. Finally, the paper is wrapped up by summarizing and concluding remarks in Section 4.

2   Model configuration and Data

2.1   WRF Model

We adopt the numerical weather prediction model WRF (version 3.8.1; Skamarock et al., 2008) to obtain fine scale and local precipitation patterns. This model allows us to dynamically downscale initial and boundary conditions, which in this study are provided by ERA5 reanalysis. To determine an optimal setup for Kenya, and particularly the Mount Kenya area, we test different parameterization schemes, focusing on cumulus parameterizations, with two different model setups and nesting ratios. The experiments are described in more detail in the following and are summarized in Table 1. The experiments are all run for the same period of time, i.e., the year 2008, except for a single experiment, which is repeated for the year 2006 to evaluate the robustness of the results for 2008 under different climate conditions. To permit the soil and the atmosphere to adjust to

the initial conditions, we allow for two month of spin-up. Since the soil variables are well equilibrated in the ERA5 data, the used spin-up time of two month in our simulations is enough to bring the soil and the atmosphere into an equilibrium. Previous studies (Angevine et al., 2014; Jerez et al., 2020; Velasquez et al., 2020) back-up the idea that rather short spin-up periods are enough for variables such as temperature or precipitation to reach the equilibrium in WRF, but for soil moisture longer periods are recommended (a few months). This means that the simulations start on the 1st of November 2007 and end on the 31st of December 2008.

Two different nesting ratios, i.e., 1:3 and 1:5, have been used in different model domain settings, to estimate the effect of the nesting ratio on the modelled precipitation and temperature (see Figure 1). For the nesting ratio of 1:3, a four domain (i.e., 27, 9, 3, 1 km horizontal resolution) and a three domain (i.e., 9, 3, 1 km horizontal resolution) setup have been tested. Also the 1:5 nesting ratio is run with two different setups, i.e., a three nested (25, 5, 1 km horizontal resolution) and a two nested domain setup (5, 1 km horizontal resolution). To test if the coarser setups affect the representation of precipitation and temperature over the study area, simulations with a coarser and finer parent grid are performed. This is because for the coarser setups the downscaling resolution is very similar to the one of ERA5, which provides the initial and boundary conditions. Such coarse spatial resolutions in the outermost domains are tested also because the final goal is to apply the WRF setup to climate simulations, which normally have a coarser resolution (around 100 km) than reanalysis data (around 30 km for ERA5). In that case, a climate simulation with a parent domain starting at 9 or 5 km is not possible. Nevertheless, the parameterizations are tested using ERA5 as boundary condition in order to be able to compare the simulations against observations of the year 2008. Note that in the simulations with a reduced number of nests (3 domains instead of 4 for the 1:3 ratio, and 2 instead of 3 for the 1:5 ratio), the parent domain always corresponds to the second domain of the experiment with one nest more (Table 1). All simulations have 49 vertical eta levels up to 50 hPa and an innermost domain located over Mount Kenya with 1 km horizontal resolution. When comparing the different sensitivity experiments in the results (section 3), the focus is always on the innermost domain of all the simulations. To save some computational costs, an adaptive time step is used, which is between 54 and 810 seconds in the outermost domain for the 1:3 ratio experiments and between 50 and 750 seconds for the 1:5 ratio. For the smaller domains, the time steps are reduced by the factor of the nesting ratio. A small sensitivity test, starting the simulation twice from the same restart file, indicates that the simulation is reproducible also with an adaptive time step.

Different physical parameterization schemes have been tested to optimize the representation of precipitation over Kenya. Tests have been done, by varying the cumulus, the long-wave (LW) radiation and the planetary boundary layer (PBL) parameterization schemes. For cumulus parameterization the Kain-Fritsch (Kain, 2004) and the scale-aware Grell-Freitas ensemble (Grell and Freitas, 2014) schemes have been used in the domains with resolutions > 5 km, and one experiment is performed without using any cumulus parameterization in all the domains. Note that the cumulus parameterization is switched off in all experiments for domains with horizontal resolutions ≤ 5 km. The LW radiation scheme has been varied between Rapid Radiation Transfer Model (RRTM; Mlawer et al., 1997) and Community Atmosphere Model (CAM; Collins et al., 2004). The two first-order non-local closure PBL schemes of Yonsei University (Hong et al., 2006) and the second version of the Asymmetric Convection Model (Pleim, 2007) have been tested. Table 1 provides a summary of the used parameterizations for each experiment and the exact setting can be found in the namelist files on Zenodo (see Code and data availability section). The

rest of the parameterization options are kept constant throughout the different experiments, i.e., WRF Single-moment 6-class scheme (Hong and Lim, 2006) for microphysics, Dudhia short-wave (SW) scheme for the SW radiation (Dudhia, 1988) and

160 the Noah–MP land surface model (Niu et al., 2011; Yang et al., 2011) to describe surface processes. In all the simulations the lake model is turned on. The 1-D physically based lake model (Subin et al., 2012) helps to simulate lake internal processes and interactions at the surface of the lake with the atmosphere (Gu et al., 2015). It increases the eddy diffusivity and thus, it strengthens also the heat transfer in the lake column (Gu et al., 2015). This is considered to be beneficial for the description of the lake surface temperature, which again helps to better represent evaporative effects and thus precipitation over the lake

165 and in the surrounding areas. A comparison of one simulation with the lake model turned off and one including the lake model reveals that the lake model is slightly beneficial for representing temporal and spatial precipitation patterns around Mount Kenya. Hence, the experiment without lake model is not presented in the following analysis, and the lake model is switched on in all the simulations. Please note that the aforementioned parameterization options are selected from an even larger set of experiments not included in this paper, tested with one nesting ratio and with four nested domains only.

170 As already shown in Table 1, each experiment obtained a name, chosen based on the area used in the literature or on the main parameterizations that it employs. The "Europe" experiment is based on the parameterization options used with WRF over Europe in previous studies by the authors (Messmer et al., 2017), but including some updated schemes such as the Noah-MP land surface model. "South America" is based on the parameterizations used for the optimal simulation of storms over the central Andes (Zamuriano et al., 2019). The remaining "Cumulus" experiments are similar to the configurations applied

175 over East Africa in previous studies (Pohl et al., 2011; Otieno et al., 2019), but they include the updated Noah-MP land surface model, and changes in the cumulus scheme option (option 3 in WRF - "Cumulus3" experiment) or no use of cumulus parameterizations at all ("No Cumulus"). The "No Cumulus" experiment is motivated by a recent study (Vergara-Temprado et al., 2020) which shows some improvements in resolving convective precipitation explicitly compared to parameterized convection in horizontal resolutions of around 25 km. The difference between the "Cumulus3" and "Cumulus3 1-way" is the

180 communication between the parent and the respective child nest. In the one-way nested options, results from the inner domain are not overwritten on the parent grid, while this is the case for two-way nested domains. Note that the two domain simulation starting at 5 km horizontal resolution is equal for the "Cumulus3 1-way" and the "No Cumulus" experiment, as they differ only in the cumulus parameterization. As in that particular simulation both explicitly resolve convective processes, the simulations are identical and will be presented as "Cumulus3 1-way".

185 ## 2.2 ERA5

ERA5 is the latest reanalysis provided by the European Centre for Medium-Range Weather Forecasts (ECMWF). At the moment, it is available from January 1979 until three months before present (Copernicus Climate Change Service (C3S), 2017). ERA5 provides different variables on the surface and various pressure levels with an hourly output. Nevertheless, we use 6-hourly data for our boundary conditions. The data are available globally on a 0.25° horizontal grid spacing and it is using

190 137 vertical model levels. A vast number of observations and satellite data are assimilated to the ERA5 gridded data using the

integrated forecasting system cycle 41r2. 24 vertical pressure levels were fed to WRF (1000, 925, 900, 850, 800, 775, 750, 700, 650, 600, 550, 500, 450, 400, 350, 300, 250, 200, 150, 100, 50, 30, 20, 10 hPa).

As stated before, our analysis will focus only on the year 2008 although 2006 is used to test the performance of the best setting with another year. Compared to the climatology of Kenya for the year 1981–2010, year 2008 is one of the warmer years, but when considering the constant warming since the beginning of the current millennium, it can be considered as a new normal (Fig. 2a). The analysis of the detrended data also supports this (not shown). In terms of precipitation, 2008 is on the dry side compared to the climatology (Fig. 2b), but it is a year with two clear rainy seasons, the 'long rains' and the 'short rains' (Fig. 2c). Additionally, the year 2006 is selected as it is rather wet compared to the year 2008.

2.3   Observational data sets

To analyse the output of the WRF simulations and to identify the best parameterization options, the downscaled product must be compared to some independent observational data sets. Hence, the precipitation results are compared to ERA5, three satellite based data sets and independent weather station measurements. For temperature, the results are compared to ERA5. A comparison to the temperature data of Climatic Research Unit data has also been performed, but the patterns are very similar to ERA5 and are therefore not shown here. Please note that the gridded data sets are bi-linearly interpolated (Climate Data Operator (CDO); Schulzweida, 2019) to the grid of the WRF domain that it is compared to, and the nearest point to the station is considered afterwards. Consequently, small differences can appear in the values related to the gridded observational data sets. However, when the pattern correlation is calculated against gridded data sets, the grid of this data set is taken as a reference and the WRF simulations are bi-linearly interpolated to that grid. In the following, the different products are described in more detail.

2.3.1   Tropical Rainfall Measurement Mission (TRMM)

The Tropical Rainfall Measurement Mission (TRMM) comprises several data sets based on satellite data, and it is provided by NASA and the Japanese Aerospace Exploration Agency (JAXA). In this study we use the gridded data product TRMM 3B42 for precipitation estimates. Note that we use the research-grade TRMM 3B42 and not the near real time version, as the first is considered to be more suitable for research (Liu, 2015). Version 7 of TRMM 3B42 is a combined product and merges satellite rainfall estimates with gauge data. To obtain the 3-hourly precipitation estimates, radars are calibrated to the microwave imager precipitation, which should result in a 3-hour microwave-only best estimate. In a next step, infrared precipitation is calibrated to the microwave product to fill regional gaps. Finally, the 3-hourly estimate is summed up to monthly values and re-calibrated using a rain gauge analysis (Huffman et al., 2007, 2010). This monthly surface precipitation gauge analysis is obtained from the Global Precipitation Climatology Centre (GPCC). The result is a Level 3 product with 3-hourly temporal and $0.25° \times 0.25°$ spatial resolution on a quasi-global (50° N – 50° S) grid. With this resolution the TRMM 3B42 data is very similar to ERA5. TRMM 3B42 is available for the period 2000-02-29 to 2020-01-02.

2.3.2 IMERG

The Integrated Multi-satellitE Retrievals from GPM (IMERG) provides a multi-satellite product, currently available in the 6th version. It is the successor of the TRMM data set. Several products with different latency periods are available, but for this study we make use of the final product, which is suitable for scientific purposes. Similar to TRMM, several microwave measurements are used to estimate precipitation, and it is further calibrated against instrument products. The half hourly precipitation estimates are further recalibrated with a CMORPH Kalman filter and the PERSIANN Cloud Classification System artificial neural network. The product is finally adjusted to the monthly GPCC rain gauge measurements and is available in half-hourly time steps and on a spatial resolution of $0.1° \times 0.1°$ (approximately 10 km $\times$ 10 km). The available time period is from June 2000 until present.

2.3.3 CHIRPS

The Climate Hazards group Infrared Precipitation with Stations (CHIRPS V2.0) provides a high-resolution data set with daily rainfall amounts (Funk et al., 2015). The $0.05°$ spatial resolved data are available for parts of the mid-latitudes and the tropics ($50°$ S – $50°$ N). The data set is generated using thermal infrared precipitation products from different institutions. To calibrate global cold cloud duration rainfall estimates, the Tropical Rainfall Measuring Mission Multi-satellite Precipitation Analysis version 7 (TMPA 3B42 v7) is used (Funk et al., 2015). In a first step, the World Meteorological Organization's Global Telecommunications System (GTS) rain gauge data, which are relatively sparsely available, are combined with cold cloud duration derived precipitation estimates. In a second step, the best available weather station data are combined with cold cloud duration based precipitation to get a product that on a monthly mean is similar to those produced by the GPCC or the Climate Research Unit from the University of East Anglia (Funk et al., 2015). Note that also IMERG and TRMM recalibrate their monthly output to results obtained from GPCC, and hence, the three data sets used for the model verification are not fully independent of each other, especially not when monthly sums are investigated.

2.3.4 Weather station data

Compared to other tropical areas in Africa, Kenya and especially the area around Mount Kenya is covered by a comparably large number of weather station data with long precipitation measurement series. Many of these measurement series are maintained by farmers. Thanks to the support and involvement of the University of Nairobi and Bern, these series are still available today (Gichuki et al., 1998; Liniger et al., 2005; MacMillan and Liniger, 2005). In addition to private stations, there are also some that are operated by the government of Kenya, i.e., the Kenya Forest Service or the Kenyan Meteorological Department. We use data of 28 stations for precipitation which have been quality controlled by Schmocker et al. (2016). Table 2 provides some information on the stations used in this study, but for more detailed information the reader is referred to Table 1 in Schmocker et al. (2016). The station ID in both tables are identical to ease comparison. We obtained four stations with temperature records from the Social Hydrological Information Platform (SHIP), associated with the Water and Land Resources Centre (WLRC) project of the Centre for Training and Integrated Research In ASAL Development (CETRAD). Three additional stations for

precipitation and temperature are included in the World Weather Records (WWR) database from the World Meteorological
Organization (WMO). These are the three first lines of Table 2. Note that the weather station data have not been adjusted to
the height of the model topography as the differences in height are in the range of a few meters. The maximum difference
between the station and model height is around 60 meters and hence the maximum discrepancy between station and modelled
temperature is around 0.4 °C, if we consider the standard environmental lapse rate of 6.5 K/km (Barry, 2008). Additionally,the
quality control performed by Schmocker et al. (2016) suggests that several stations are only suitable for monthly analyses. As
the number of stations in the innermost domain should stay as large as possible, the study is mainly based on the monthly
resolution. Most of the weather stations are located on the northwestern slopes of Mount Kenya and they are rather scarce to
the southeast of it, which can affect the reliability of our results. However, we reduce this uncertainty by comparing our results
also against several gridded observational data sets.

3 Results

3.1 Sensitivity of Precipitation

3.1.1 Temporal analysis

To investigate the sensitivity of simulated precipitation due to different parameterization options of the WRF model, we first
show the annual cycle based on monthly means. Thereby, the sensitivity simulations with WRF and the three gridded observa-
tional data sets are compared to in-situ data from weather stations (see Table 2 for more details). To compare gridded data with
point measurements at weather stations, the grid point that is closest to the corresponding latitude and longitude of the weather
station is considered in the WRF simulation and the gridded observations. Two performance measures for each weather station
are calculated and summarized in box-whisker plots (Fig. 3): the temporal correlation and the root mean squared error (RMSE).
For correlations, we use the Spearman correlation, which is a rank correlation, that is suitable for the small sample sizes that are
explored here. Additionally, the standard deviation of each data set is compared to the one extracted from the weather stations
(not shown). Several different gridded observational data sets are employed here to compare the sensitivity simulations and to
classify which WRF setting performs best. As not only the weather station data but also the gridded observational data sets are
subject to a range of uncertainties, we do not only rely on one product. Note that because the gridded data sets are bi-linearly
interpolated to the respective WRF grid small differences can appear in the values of temporal correlations and RMSEs of each
set-up and hence, also the shape of bars corresponding to these data sets in the box-whisker plots can look slightly different.

The temporal correlations show that the observational data sets, ERA5, TRMM and especially IMERG, are well correlated
(Fig. 3a). This is expected as the data are not fully independent from each other. IMERG has the best correlation with the highest
median but also with the smallest spread. This is true for all the different nesting options, but especially the WRF setting with
a parent grid of 27 km and 4 domains shows a correlation of around 0.8 in the median value for all the observational data sets.
The fact that IMERG and the weather station data show such a good agreement further confirms the quality of the latter. The
temporal correlations of the sensitivity simulations show a strong dependence on the nesting options. The simulations with

fewer nests (right part of Fig. 3a) exhibit a higher correlation and a smaller spread than the two simulations that have one additional nest (left part of Fig. 3a). In particular, the "No Cumulus" simulation, but also the "Europe" parameterization, show a poor performance in the temporal correlation. Note that the poor performance of the "No Cumulus" can only be observed in nesting options with a larger number of domains, i.e., setups with a parent grid of 27 or 25 km. The fact that the nesting option

290 is important here suggests that with fewer domains (only 3 instead of 4 nests for the 1:3 ratio, and 2 instead of 3 for the 1:5 ratio), the simulation in the innermost domain is still more strongly influenced by the boundary conditions of the driving data, i.e., ERA5. Thus, the simulations with fewer nests cannot evolve with the same freedom as the ones with more nests, resulting in a better temporal agreement of the simulations. This is especially clear in the "No Cumulus" simulation.

While all the gridded observational data sets yield a rather high temporal correlation, the RMSE of ERA5 is rather high

295 compared to the ones of TRMM, IMERG and CHIRPS (Fig. 3b). A reason for this is that the precipitation in ERA5 is independent of the weather station data, as precipitation is not assimilated into this product. Otherwise the RMSE shows similar results as the correlations for both the gridded observations as well as the sensitivity simulations. Hence, the parameterization of the simulation is only of minor importance compared to the nesting options. Similar findings are obtained when using the standard deviation (not shown). Here, the WRF simulations are generally within the range of the standard deviation observed

300 in the weather station data, except for the "Europe" parameterization in the nesting options with fewer nests. In that case, the standard deviation is strongly underestimated indicating that the variability of precipitation is not fully captured. Additionally, the standard deviations of the gridded observational data sets are smaller than the ones of the weather station data, which is owed to the coarser resolution of the first. At finer temporal resolutions than monthly sums, these temporal correlations and RMSEs reproduce the differences between the experiments as discussed for monthly means. However, using finer time scales

305 leads to a general reduction of the correlation coefficients and an increase in RMSEs. This is expected, as the variability is higher and because it is more and more challenging for the model to capture the exact timing of precipitation (not shown).

3.1.2 Pattern correlation analysis

Since the temporal correlation and the RMSE do not clearly define which parameterization option of WRF delivers the best results for precipitation in the region around Mount Kenya, we investigate the pattern correlation of the simulations compared

310 to weather station data in a first step and to the gridded observational data set CHIRPS in a second step. Figure 4 shows in the first row the pattern correlation between the WRF-simulations and the weather station data for each month. The different columns indicate different parameterization options and the symbols within each panel shows the nesting option. The black vertical line in each panel is equal to a correlation coefficient of 0.5. This value is a moderate correlation and still explains roughly 25 % of the variance, but it is a visual support to determine more easily which simulations and nesting options perform

315 better than others. The number of months that are equal or exceed this limit of 0.5 in correlation are counted and summed up in the table below each panel ('# months' column).

The gridded observational data sets agree reasonably well in terms of the spatial pattern of precipitation, except for ERA5. The fact that ERA5 shows a poor correlation with the weather station data is because the domain is located over steep terrain, where a high resolution is needed to resolve precipitation patterns appropriately. CHIRPS has the highest spatial resolution

320 and shows a slightly better pattern correlation than IMERG (especially also in June) and hence, we have decided to compare the WRF-simulations also against the CHIRPS gridded data set (second row of Fig. 4). Additionally, CHIRPS shows high correlations and low RMSEs in the temporal analysis. Similarly to the temporal correlation, the simulations with fewer nests obtain a better pattern correlation compared to the ones with an additional nest. The "South America" and the "No Cumulus" parameterizations show the highest agreement with the weather station data for the nesting options that have an additional nest,

325 while clearly the "Cumulus3 1-way" option is the best one of the simulations with fewer nests. Overall, the simulations have a better performance in the rainy seasons MAM and ON, while the dry months (and in particular June) are not very well captured by the model simulations.

Besides the comparison to the weather station data, the simulations and gridded observational data are compared to CHIRPS (see second row of Fig. 4). As mentioned before, all the simulations were bi-linearly interpolated to the grid of CHIRPS for

330 this spatial analysis. The gridded observational data sets perform well compared to CHIRPS (including also ERA5). Again this is expected as the data are not fully independent. The pattern correlation of the WRF simulations compared to CHIRPS are rather high in all the simulations. No clear difference between the different nesting options are evident. The "South America" and the "No Cumulus" options show the best agreement with CHIRPS in precipitation patterns, but also "Cumulus3 1-way" performs well. The "Europe" parameterization is clearly the worst, even if it shows one of the highest correlations in the dry

335 months June and July. This is because the "Europe" parameterization setup produces rather dry conditions over Africa and hence, the dry months are better represented compared to the others that simulate generally wetter conditions.

3.1.3 Annual cycle

To further understand how well the different parameterization and nesting options are able to represent precipitation around Mount Kenya, the annual cycle is plotted as grid point averages of monthly precipitation sums of the innermost domain (1 km;

340 Fig. 5). Please note that the gridded observational data sets do not obtain exactly the same values for the different nesting ratios 1:3 (first row) and 1:5 (second row), as the domain sizes are not exactly equal. The innermost domain in the 1:5 nesting ratio setup is slightly bigger. The three gridded observational data sets TRMM, IMERG and CHIRPS agree well and are considered as the reference here, as they show a good temporal and pattern correlation with the weather station data. This is true except for November, when CHIRPS records a much higher value in precipitation amounts than TRMM and IMERG. As CHIRPS

345 shows one of the weakest pattern correlations in November compared to the weather station data, IMERG and TRMM should be considered as the reference in this month. ERA5 does also agree, but the 'long rains' (MAM) have the peak intensity a bit too early, while the intensity in the 'short rains' (ON) is too intense on average. For the dry months, ERA5 also overestimates precipitation compared to the other gridded observational products. Overall the gridded data sets come up with similar annual precipitation sums (see the inset of Fig. 5), except for ERA5, which shows a slight overestimation in annual precipitation

350 sums. Comparing the monthly precipitation sums of the sensitivity simulations with the gridded observational reference, we find again that the "Europe" parameterization option is not well suited for this area as it is not able to capture correctly the two rainy seasons near Mount Kenya. The 'long rains' show a clear deficit in precipitation, while the outcome of the 'short rains' strongly depends on the number of nests. With fewer nests the 'short rains' are also clearly underestimated, but with an

additional nest precipitation is either almost correct or overestimated. The differences between the "Europe" parameterization and the others are the long wave radiation and the PBL parameterization, which are both responsible for the reduction in precipitation amounts, according to previous sensitivity tests with these parameterizations (not shown). The "No Cumulus" setup performs well in both wet seasons, but it overestimates precipitation during the dry season. The "Cumulus3" options show a clear sensitivity of the precipitation amounts in the 'long rains' to the number of nests, with a much better representation with fewer nests. In the 'short rains', the "Cumulus3" options follow the curve of CHIRPS and therefore shows an overestimation. The fact that the "Europe" setting is not suited for this regions becomes even clearer by including the annual precipitation sums. Except for the 25 km parent grid, the "Europe" setting captures only around 50 % of the annual precipitation, and hence, it clearly underestimates the water availability. All the other settings perform similarly well on an annual basis (insets in Fig. 5). It is further noteworthy that the WRF model with the "Cumulus 3" options is able to correct the overestimation obtained by ERA5, which is the driving data set of the simulations.

3.1.4 Precipitation patterns

Another measure used to identify the best setup of WRF for this region are the precipitation patterns of the WRF simulations. Due to the aforementioned motivation to use the tested settings in a climate simulation, in the following, the simulation of the innermost domain (D4; 1 km) with the parent domain of 27 km horizontal grid spacing and a nesting ratio of 1:3 is presented. Note that the simulations with a 25 km parent grid and a nesting ratio of 1:5 show similar results and hence, are not shown here. To present the results months within the three main seasons are presented, i.e., the 'long rains', 'short rains' and the dry season. April (Fig. 6a) is chosen as it is in the midst of the 'long rains'. November (Fig. 6b) is selected as it is within the 'short rains' and has a larger spread between the different experiments than October, and finally June (Fig. 6c) represents a month in the dry season and shows stronger deviations compared to station data. As CHIRPS is the data set that shows the best agreement with the weather station data (as shown in Fig. 4), and because it also shows the highest resolution and detail, in the following only this gridded observational data set is presented as reference. Additionally, the "Europe" experiment is discarded because of its weak performance in the previous analyses.

In April, the precipitation from CHIRPS is similar to the measured amounts of precipitation, with the exception of a small region located to the north of Mount Kenya where precipitation is overestimated by this gridded data set (Fig. 6a). Bearing in mind that also the observational data set is subject to some uncertainties, the "South America" parameterization shows similar precipitation amounts and pattern along a diagonal band from southwest to northeast, lacking some of the precipitation southeast of Mount Kenya, as indicated by CHIRPS. The northern part of the domain seems to be to dry compared to CHIRPS, but stations along the northern slope of Mount Kenya agree relatively well. The other three options manage to produce a precipitation pattern as observed in CHIRPS. Nevertheless, the "No Cumulus" parameterization is too wet especially in the northwestern part of the domain, and the steep gradient from high precipitation rates in the vicinity of Mount Kenya to dryer conditions to the northwest of it is not well captured. The two "Cumulus3" parameterization options capture this pattern the best, including also some finer details along the right and bottom boundaries of the domain.

CHIRPS is capturing the precipitation pattern also quite well in November, with some deviations compared to the weather station data south and northwest of Mount Kenya (Fig. 6b). " South America" captures the precipitation amounts of the stations quite well, but the pattern shows some deviations compared to CHIRPS, especially in the northwestern corner of the domain. The two "Cumulus3" and the "No Cumulus" options are able to capture the patterns well with some overestimation in the simulations driven by the first option and a slight underestimation in precipitation amounts for the latter parameterization option. Given the uncertainty range within the observation based data, it cannot be expected that a single sensitivity simulation can agree with all the stations or with one of the gridded observational data sets.

June is clearly much drier than April and also CHIRPS records too much precipitation compared to the weather station data (see Fig. 6c). Given the uncertainty range of the observation based data, the "South America" parameterization option does not fully agree with CHIRPS in terms of the general pattern, as no dry corridor in the east is simulated and precipitation is overestimated at most of the stations. This is also true for the "No Cumulus" parameterization option, but here the pattern agrees better, with a clear overestimation in precipitation amounts. "Cumulus3" and "Cumulus3 1-way" again result in the best pattern rendering it difficult to choose between the two, as some stations are better in one and other stations are better described in the other setting. Since one-way nesting does not overwrite the solution of the corresponding parent grid, this option should be preferred over the two-way nesting option. It allows to not only focus on the innermost domain, but also investigations of a larger scale picture are able without any disturbances within the domain.

All the WRF simulations reasonably resemble the precipitation pattern over Mount Kenya in the year 2008. The "Europe" setting provides the worst performance and throughout the whole year too dry conditions. The "No Cumulus" parameterization and the "Cumulus3" options provide throughout the analysis the best performances. The fact that the "No Cumulus" option is generally too wet allows us to define the "Cumulus3 1-way" option as the best for our purpose. Note also that the "No Cumulus" parameterization option produces a patchy picture in the outermost domain with monthly sums, which is a clear sign of a structural problem, i.e., convection is induced always at the same location (not shown), which is rather unrealistic. Hence, this simulation is also not suitable for a larger scale analysis of precipitation and precipitation changes in a warmer climate. Nevertheless, it must be noted that peak precipitation rates on a sub-daily basis are captured much more realistic with respect to IMERG, compared to the other parameterizations options, but only in domains where the others use a cumulus parameterization (see supplementary Fig. S1).

3.1.5 Evaluation of performance under wet climatic conditions: year 2006

With the best parameterization option "Cumulus3 1-way" and the setup with a parent domain of 27 km horizontal grid spacing and a nesting ratio of 1:3, a further experiment is performed, in order to test the applicability to other years. Therefore, the rather wet year 2006 is selected, as indicated in Fig. 2b. Here, we do not compare to TRMM anymore, as IMERG and CHIRPS provide finer resolved precipitation information. The temporal correlation of monthly precipitation sums with respect to the station data (see supplementary Fig. S2a) is even slightly higher in 2006 than in 2008, while ERA5 performs worse in 2006 than 2008. CHIRPS and IMERG perform similarly in both years. The RMSE of all the different analysed precipitation data is slightly larger than in 2008, but shows still a good performance (see supplementary Fig. S2b). Both CHIRPS and IMERG

show a similarly good pattern correlation with the station data in 2006 as in 2008. ERA5 shows also a similar behaviour in the two years, being not able to capture the main precipitation pattern of the stations. "Cumulus3 1-way" reflects the precipitation pattern against weather station data reasonably well (see supplementary Fig. S2c), with 7 months of higher correlations than 0.5, which is a clear improvement compared to 2008. The spatial pattern correlation with respect to CHIRPS (see supplementary Fig. S2d) results in values higher than 0.5 in 11 months, which none of the parameterization experiments reached in the year 2008. Only December is just below this limit with a spatial correlation of 0.476.

"Cumulus3 1-way" captures the precipitation patterns (see supplementary Fig. S3) well especially in the two rainy seasons of 2006, i.e., April and November. In April the northern part of the domain is a bit too dry compared to the stations and CHIRPS, while in November the eastern part is slightly too dry compared to CHIRPS, but also compared to the station data. In June, CHIRPS and WRF produce very similar patterns, but compared to the station data they are both too wet, especially on the northern foothills of Mount Kenya. All in all, this setting shows even a better performance in the wet year 2006 than in the slightly dry year 2008.

3.2 Sensitivity of Temperature

Once we have investigated the sensitivity of simulated precipitation due to different parameterization options, we focus on temperature. To do so, the sensitivity simulations with WRF, except for "Europe" because of its bad performance in precipitation, are compared to the driving reanalysis ERA5 and the in-situ data from weather stations (see Table 2 for more details). To measure how the different settings simulate the temperature near Mount Kenya, the 2-metre temperature patterns are evaluated. The same months as for precipitation are selected for temperature: April (Fig. 7a) and November (Fig. 7b), within the 'long' and 'short rains' respectively, and June (Fig. 7c), within the dry season. In order to highlight the differences between the sensitivity experiments, only the absolute values of the gridded data sets and the "Cumulus3 1-way" experiment are depicted. For the remaining sensitivity experiments, the anomalies compared to our best setting experiment are presented.

ERA5 temperature serves as boundary and initial conditions for the WRF simulation. Given this constraint, we expect a better representation of the simulated 2-metre temperature than of precipitation. Also, the region of interest is dominated by steep topography, which is directly related to temperature and consequently, strong gradients of temperature are expected near Mount Kenya.

It is not surprising that ERA5 represents temperature relatively similarly and independently of the season (rainy or dry) as Kenya is located at the equator. ERA5 describes the orography of the domain clearly and most of the few weather station data agree well with ERA5, but the WRF simulation "Cumulus3 1-way" produces a better temperature profile, which is mainly owed to the better resolution and a more detailed characterization of the topography.

In April (Fig. 7a), the two "Cumulus3" simulations have a very similar representation of temperature, as the only difference is the communication between the nests. The difference for the "South America" experiment is mainly in the range of $\pm 0.5\,^{\circ}$C, with positive anomalies over Mount Kenya and negative anomalies in the surrounding plains. In the case of the "No Cumulus" parameterization, strong negative anomalies are observed over the entire region, particularly in the southeastern corner of it where anomalies reach $-2\,^{\circ}$C. This negative temperature anomaly is probably related to the overestimation in precipitation

as most of the domain obtains more precipitation than in the "Cumulus3 1-way" simulation. This excess in water can be transformed into latent heating through evaporation and can contribute to a cooling effect over the domain.

In November the "Cumulus3 1-way" option overestimates the precipitation somewhat, which generally results in cooler temperatures compared to observations in some stations (e.g., station 1 and 4 in Fig. 7b). As the other sensitivity experiments simulate a drier monthly climate especially in the plains, a positive temperature signal is found in these areas as well. Generally, the temperature differences between the experiments are again rather small and below 1 °C.

The two "Cumulus3" options are able to simulate correctly the observed temperature in June (Fig. 7c), and their differences are rather small (below ± 0.25 °C). The temperature bias for the "South America" experiment is higher in June than in April, but the patterns are similar (positive anomalies over Mount Kenya, but negative ones in the plains). Again, negative anomalies are simulated in the "No Cumulus" experiment, which could also be related to an increase in precipitation amounts, especially in the southeastern corner of the domain.

As described above, the differences in the patterns in the three months resemble to some extent the differences in precipitation, i.e., where more precipitation is simulated compared to "Cumulus3 1-way", temperatures are reduced. One process which partly explains this is the transformation of energy into latent heating through evaporative processes. Where precipitation is comparably reduced to the "Cumulus3 1-way" parameterization, a warming is found. This is potentially due to energy that is transformed into sensible heating. Additionally, moisture advection but also small differences in the description of cloud cover are additional relevant processes explaining some of the changes in temperature.

4   Summary and Conclusions

The goal of this study was to find a setup for WRF in order to realistically simulate precipitation patterns and amounts over and around Mount Kenya at a kilometer scale. This task is challenged by the fact that this region has a complex topographic structure and is influenced by large-scale circulation controls, which leads to heterogeneous precipitation patterns. As this is one of the first studies to resolve Mount Kenya region at such fine scale, different parameterization options and combinations must be tested to obtain an optimal result for this area. We employ the WRF model and experiment with different combinations of cumulus (Kain-Fritsch, Grell-Freitas, no cumulus), LW (CAM, RRTM) and PBL (ACM2, YSU) parameterizations, but also with the number of nested domains and nesting ratios (1:3 and 1:5). The different simulations are not only compared to different gridded observational data sets, such as IMERG, TRMM and CHIRPS, but also to a large number of weather station data operated by private farms, CETRAD and the Kenyan government.

Correlating the annual cycle as monthly sums reveals that the gridded observations and the weather station data agree very well, indicating that the here presented weather station data are reliable. The temporal correlations further lead to the conclusion that if ERA5 is used as boundary conditions in a smaller and higher resolved domain (i.e., simulations with one less nest) the simulation is more constrained and hence, the temporal correlation is better with a reduced number of nests. This result is mainly important for simulations driven with reanalysis data, as they capture most of the atmospheric circulation and processes well and therefore are reliable, which is not necessarily true for climate simulations as well. The "No cumulus"

parameterization scheme is especially sensitive to changes in number of nests in terms of temporal correlation. Concerning the nesting ratio, we are not able to distinguish between the two options, so any of the two are able to produce realistic results.

490 Also important for water availability in the area around Mount Kenya are the precipitation patterns and amounts. The objective pattern correlations indicate that also fewer nests result in a better spatial correlation, but when comparing against the most accurate gridded data set, CHIRPS, there is not much difference between the number of nests in spatial patterns. Compared to the temporal correlation, the "No Cumulus" parameterization results in rather accurate pattern correlations. The pattern correlation is not only a valuable tool to evaluate the sensitivity simulations, but also the gridded observational data sets.

495 The comparison to the weather station data reveals that CHIRPS yields a pattern closer to the weather stations. One important factor for this result is certainly the nominal resolution of the data, as CHIRPS reveals the finest precipitation structure of all the gridded observational data sets.

The "Europe" configuration obtains not only one of the worst temporal, but also pattern correlation. The actual patterns within the innermost domain reveal that the "Europe" configuration is clearly too dry, both in the rainy and the dry seasons.

500 The underestimation in precipitation can be attributed to both the LW and PBL parameterizations. But not only the precipitation amounts are underestimated, also the precipitation pattern is not fully captured. The "South America" setting is more accurate when it comes to monthly precipitation sums in the rainy season, but it clearly has a wet bias in the dry season, and also the precipitation pattern is missing some details compared to CHIRPS. While the two "Cumulus3" options and the "No Cumulus" option provide rather good precipitation patterns, the latter clearly overestimates the monthly sums. Hence, we conclude that

505 the "Cumulus3 1-way" option is the best parameterization setting in WRFV3.8.1 for the area around Mount Kenya. The 1-way nesting option is preferred over the 2-way option, as the latter affects the representation of the domain when cumulus parameterization is turned off. Hence, with the 1-way option, all domains and scales of the simulation can be integrated into the analysis.

The "Cumulus3 1-way" setting provides even better results for the year 2006, not only in terms of temporal correlations, but

510 also pattern correlations and precipitation amounts show a good agreement with respect to CHIRPS and to the weather station data. This result further supports the robustness of the here presented results, as not only rather dry years but also very wet years are reasonably well captured by this WRF model setup and driven with ERA5.

Similar to other studies, we also find an overestimation in precipitation compared to observations (Cook and Vizy, 2013; Williams et al., 2015). Nevertheless, with our sensitivity experiments we identify a parameterization setting that represents

515 precipitation amounts rather well in the rainy seasons, while a wet bias remains in the dry season. Certainly, the very high resolution of our simulations helps to better represent not only the pattern of precipitation, but also of temperature, resembling findings of Kerandi et al. (2017). It is not surprising that a high resolution can add value in the representation of precipitation and temperature, as this region is located within complex topographic structures.

Having found the optimal setting for the Mount Kenya area, climate change simulations can be performed. These allow to

520 get a detailed picture of the climate sensitivity in this area and the possible changes in water availability and the actual warming in the area. Next steps also include sensitivity experiments to land use changes. This will help to understand how future changes in agriculture will affect water availability in the flat lands around Mount Kenya.

Code and data availability.   The Weather Research and Forecasting (WRF) model V3.8.1 is freely available online and can be downloaded from the users' page: https://www2.mmm.ucar.edu/wrf/users/download/get_sources.html. All the namelist files necessary to reproduce the simulations performed in this study, and the codes created by the authors to read, analyse and plot the results included in this paper are available within a zip file that can be downloaded from: https://doi.org/10.5281/zenodo.4090589. Additionally, this link also includes the postprocessed outputs for precipitation and temperature from our WRF sensitivity experiments. All the observational gridded data sets for precipitation included in this study are freely available online. TRMM and IMERG can be downloaded from the Earth Observing System Data and Information System (EOSDIS) from NASA (https://doi.org/10.5067/TRMM/TMPA/3H-E/7 and https://doi.org/10.5067/GPM/IMERG/3B-HH/06 respectively), and CHIRPS can be download from the Climate Hazards Center of the UC Santa Barbara (https://doi.org/10.15780/G2RP4Q). The weather station data from WMO used in this study can be downloaded from the World Weather Records website (https://www.ncei.noaa.gov/access/search/data-search/global-summary-of-the-day). The data from the stations maintained by CETRAD in Kenya can be downloaded from the Social Hydrological Information Platform (http://www.wlrc-ken.org/admin/dashboard/home).

Author contributions.   The conceptualization was developed by all the authors. The preparation of data sets and the methodology was designed by M.M. and S.J.G.-R. The analysis was carried out by all the authors. The original draft of the paper was written by M.M. and S.J.G.-R., but all the authors took part in the edition and revision of it.

Competing interests.   The authors declare no competing interests.

Acknowledgements.   The authors thank the Wyss Foundation for funding this pilot project. The authors acknowledge CETRAD, Noemi Imfeld and Stefan Brönnimann for sharing the weather station data of Kenya. Financial support by the Swiss National Science Foundation (Early PostDoc.Mobility grant: P2BEP2-181837) and the Oeschger Centre for Climate Change Research is acknowledged. The TMPA data were provided by the NASA/Goddard Space Flight Center's Mesoscale Atmospheric Processes Laboratory and PPS, which develop and compute the TMPA as a contribution to TRMM. The computational resources were provided by CSCS (roughly 750'000 CPU hours), and the authors thank the creators of the WRF model. The authors thank two anonymous reviewers for their insightful comments that have led to an improved version of the paper. Finally, some of the calculations were carried out with R (R Core Team, 2018), and the authors want to thank all the authors of the packages used for it: akima, ggplot2, latticeExtra, maptools, plotrix, reshape2, rgdal, rgeos, RNetCDF, shape and sp.

References

Angevine, W. M., Bazile, E., Legain, D., and Pino, D.: Land surface spinup for episodic modeling, Atmospheric Chemistry and Physics, 14, 8165–8172, https://doi.org/10.5194/acp-14-8165-2014, 2014.

550 Ayugi, B. O., Wen, W., and Chepkemoi, D.: Analysis of Spatial and Temporal Patterns of Rainfall Variations over Kenya, Journal of Environment and Earth Science, 6, 69–83–83, 2016.

Ban, N., Schmidli, J., and Schär, C.: Evaluation of the convection-resolving regional climate modeling approach in decade-long simulations, Journal of Geophysical Research: Atmospheres, 119, 7889–7907, https://doi.org/10.1002/2014JD021478, 2014.

Barry, R. G.: Mountain Weather and Climate, Cambridge University Press, 3 edn., https://doi.org/10.1017/CBO9780511754753, 2008.

555 Behera, S. K., Luo, J. J., Masson, S., Rao, S. A., Sakuma, H., and Yamagata, T.: A CGCM Study on the Interaction between IOD and ENSO, Journal of Climate, 19, 1688 – 1705, https://doi.org/10.1175/JCLI3797.1, 2006.

Bellprat, O., Kotlarski, S., Lüthi, D., De Elía, R., Frigon, A., Laprise, R., and Schär, C.: Objective Calibration of Regional Climate Models: Application over Europe and North America, Journal of Climate, 29, 819–838, https://doi.org/10.1175/JCLI-D-15-0302.1, 2016.

Brune, S., Buschow, S., and Friederichs, P.: Observations and high-resolution simulations of convective precipitation organization over the
560 tropical Atlantic, Quarterly Journal of the Royal Meteorological Society, 146, 1545–1563, https://doi.org/10.1002/qj.3751, 2020.

Camberlin, P. and Philippon, N.: The East African March–May Rainy Season: Associated Atmospheric Dynamics and Predictability over the 1968–97 Period, Journal of Climate, 15, 1002–1019, https://doi.org/10.1175/1520-0442(2002)015<1002:TEAMMR>2.0.CO;2, 2002.

Collier, E., M?lg, T., and Sauter, T.: Recent Atmospheric Variability at Kibo Summit, Kilimanjaro, and Its Relation to Climate Mode Activity, Journal of Climate, 31, 3875 – 3891, https://doi.org/10.1175/JCLI-D-17-0551.1, 2018.

565 Collins, W. D., Rasch, P. J., Boville, B. A., Hack, J. J., McCaa, J. R., Williamson, D. L., Kiehl, J. T., Briegleb, B., et al.: Description of the NCAR community atmosphere model (CAM 3.0), 2004.

Cook, K. H. and Vizy, E. K.: Projected Changes in East African Rainy Seasons, Journal of Climate, 26, 5931–5948, https://doi.org/10.1175/JCLI-D-12-00455.1, 2013.

Copernicus Climate Change Service (C3S): ERA5: Fifth generation of ECMWF atmospheric reanalyses of the global climate, https://cds.
570 climate.copernicus.eu/cdsapp#!/home, Copernicus Climate Change Service Climate Data Store (CDS), date of access: 2019-May-04, 2017.

Dudhia, J.: Numerical Study of Convection Observed during the Winter Monsoon Experiment Using a Mesoscale Two-Dimensional Model, Journal of the Atmospheric Sciences, 46, 3077–3107, https://doi.org/10.1175/1520-0469(1989)046<3077:NSOCOD>2.0.CO;2, 1988.

Finney, D. L., Marsham, J. H., Jackson, L. S., Kendon, E. J., Rowell, D. P., Boorman, P. M., Keane, R. J., Stratton, R. A., and Senior, C. A.:
575 Implications of Improved Representation of Convection for the East Africa Water Budget Using a Convection-Permitting Model, Journal of Climate, 32, 2109–2129, https://doi.org/10.1175/JCLI-D-18-0387.1, 2019.

Funk, C., Peterson, P., Landsfeld, M., Pedreros, D., Verdin, J., Shukla, S., Husak, G., Rowland, J., Harrison, L., Hoell, A., and Michaelsen, J.: The climate hazards infrared precipitation with stations – a new environmental record for monitoring extremes, Scientific Data, 2, 1–21, https://doi.org/10.1038/sdata.2015.66, 2015.

580 Gichuki, F. N., Liniger, H., and Schwilch, G.: Knowledge about highland – lowland interactions: the role of a natural resource information system, Eastern and Southern Africa Geographical Journal, 8, 5–14, 1998.

Giorgi, F., Torma, C., Coppola, E., Ban, N., Schär, C., and Somot, S.: Enhanced summer convective rainfall at Alpine high elevations in response to climate warming, Nature Geoscience, 9, 584–589, https://doi.org/10.1038/ngeo2761, 2016.

Gómez-Navarro, J. J., Raible, C. C., Bozhinova, D., Martius, O., García Valero, J. A., and Montávez, J. P.: A new region-aware bias-correction method for simulated precipitation in areas of complex orography, Geoscientific Model Development, 11, 2231–2247, https://doi.org/https://doi.org/10.5194/gmd-11-2231-2018, 2018.

Grell, G. A. and Freitas, S. R.: A scale and aerosol aware stochastic convective parameterization for weather and air quality modeling, Atmospheric Chemistry and Physics, 14, 5233–5250, https://doi.org/10.5194/acp-14-5233-2014, https://www.atmos-chem-phys.net/14/5233/2014/, 2014.

Gu, H., Jin, J., Wu, Y., Ek, M. B., and Subin, Z. M.: Calibration and validation of lake surface temperature simulations with the coupled WRF-lake model, Climatic Change, 129, 471–483, https://doi.org/10.1007/s10584-013-0978-y, 2015.

Hastenrath, S. and Polzin, D.: Dynamics of the surface wind field over the equatorial Indian Ocean, Quarterly Journal of the Royal Meteorological Society, 130, 503–517, https://doi.org/https://doi.org/10.1256/qj.03.79, 2004.

Hastenrath, S. and Polzin, D.: Mechanisms of climate anomalies in the equatorial Indian Ocean, Journal of Geophysical Research: Atmospheres, 110, https://doi.org/https://doi.org/10.1029/2004JD004981, 2005.

Hastenrath, S., Polzin, D., and Mutai, C.: Circulation Mechanisms of Kenya Rainfall Anomalies, Journal of Climate, 24, 404–412, https://doi.org/10.1175/2010JCLI3599.1, 2010.

Hong, S.-Y. and Lim, J.-O. J.: The WRF single-moment 6-class microphysics scheme (WSM6), Asia-Pacific Journal of Atmospheric Sciences, 42, 129–151, 2006.

Hong, S.-Y., Noh, Y., and Dudhia, J.: A New Vertical Diffusion Package with an Explicit Treatment of Entrainment Processes, Monthly Weather Review, 134, 2318–2341, https://doi.org/10.1175/MWR3199.1, 2006.

Huffman, G. J., Bolvin, D. T., Nelkin, E. J., Wolff, D. B., Adler, R. F., Gu, G., Hong, Y., Bowman, K. P., and Stocker, E. F.: The TRMM Multisatellite Precipitation Analysis (TMPA): Quasi-Global, Multiyear, Combined-Sensor Precipitation Estimates at Fine Scales, Journal of Hydrometeorology, 8, 38–55, https://doi.org/10.1175/JHM560.1, publisher: American Meteorological Society, 2007.

Huffman, G. J., Adler, R. F., Bolvin, D. T., and Nelkin, E. J.: The TRMM Multi-Satellite Precipitation Analysis (TMPA), in: Satellite Rainfall Applications for Surface Hydrology, edited by Gebremichael, M. and Hossain, F., pp. 3–22, Springer Netherlands, Dordrecht, https://doi.org/10.1007/978-90-481-2915-7_1, 2010.

Jacob, D., Bärring, L., Christensen, O. B., Christensen, J. H., De Castro, M., Deque, M., Giorgi, F., Hagemann, S., Hirschi, M., Jones, R., et al.: An inter-comparison of regional climate models for Europe: model performance in present-day climate, Climatic change, 81, 31–52, 2007.

Jacob, D., Elizalde, A., Haensler, A., Hagemann, S., Kumar, P., Podzun, R., Rechid, D., Remedio, A. R., Saeed, F., Sieck, K., and et al.: Assessing the Transferability of the Regional Climate Model REMO to Different COordinated Regional Climate Downscaling EXperiment (CORDEX) Regions, Atmosphere, 3, 181–199, https://doi.org/10.3390/atmos3010181, http://dx.doi.org/10.3390/atmos3010181, 2012.

Jerez, S., López-Romero, J. M., Turco, M., Lorente-Plazas, R., Gómez-Navarro, J. J., Jiménez-Guerrero, P., and Montávez, J. P.: On the Spin-Up Period in WRF Simulations Over Europe: Trade-Offs Between Length and Seasonality, Journal of Advances in Modeling Earth Systems, 12, e2019MS001 945, https://doi.org/10.1029/2019MS001945, 2020.

Kain, J. S.: The Kain–Fritsch Convective Parameterization: An Update, Journal of Applied Meteorology, 43, 170–181, https://doi.org/10.1175/1520-0450(2004)043<0170:TKCPAU>2.0.CO;2, 2004.

Kendon, E. J., Ban, N., Roberts, N. M., Fowler, H. J., Roberts, M. J., Chan, S. C., Evans, J. P., Fosser, G., and Wilkinson, J. M.: Do Convection-Permitting Regional Climate Models Improve Projections of Future Precipitation Change?, Bulletin of the American Meteorological Society, 98, 79–93, https://doi.org/10.1175/BAMS-D-15-0004.1, 2017.

Kerandi, N. M., Laux, P., Arnault, J., and Kunstmann, H.: Performance of the WRF model to simulate the seasonal and interannual variability of hydrometeorological variables in East Africa: a case study for the Tana River basin in Kenya, Theoretical and Applied Climatology, 130, 401–418, https://doi.org/10.1007/s00704-016-1890-y, 2017.

625 Kilavi, M., MacLeod, D., Ambani, M., Robbins, J., Dankers, R., Graham, R., Titley, H., Salih, A. A. M., and Todd, M. C.: Extreme Rainfall and Flooding over Central Kenya Including Nairobi City during the Long-Rains Season 2018: Causes, Predictability, and Potential for Early Warning and Actions, Atmosphere, 9, https://doi.org/10.3390/atmos9120472, https://www.mdpi.com/2073-4433/9/12/472, 2018.

Liebmann, B., Hoerling, M. P., Funk, C., Bladé, I., Dole, R. M., Allured, D., Quan, X., Pegion, P., and Eischeid, J. K.: Understanding Recent Eastern Horn of Africa Rainfall Variability and Change, Journal of Climate, 27, 8630–8645, https://doi.org/10.1175/JCLI-D-13-00714.1,
630 2014.

Liniger, H., Gikonyo, J., Kiteme, B., and Wiesmann, U.: Assessing and Managing Scarce Tropical Mountain Water Resources, Mountain Research and Development, 25, 163–173, https://doi.org/10.1659/0276-4741(2005)025[0163:AAMSTM]2.0.CO;2, 2005.

Liu, Z.: Comparison of precipitation estimates between Version 7 3-hourly TRMM Multi-Satellite Precipitation Analysis (TMPA) near-real-time and research products, Atmospheric Research, 153, 119–133, https://doi.org/10.1016/j.atmosres.2014.07.032, 2015.

635 MacMillan, L. and Liniger, H. P.: Monitoring and Modelling for the Sustainable Management of Water Resources in Tropical Mountain Basins: The Mount Kenya Example, in: Global Change and Mountain Regions: An Overview of Current Knowledge, edited by Huber, U. M., Bugmann, H. K. M., and Reasoner, M. A., pp. 605–616, Springer Netherlands, Dordrecht, https://doi.org/10.1007/1-4020-3508-X_60, 2005.

Messmer, M., Gómez-Navarro, J. J., and Raible, C. C.: Sensitivity experiments on the response of Vb cyclones to sea surface temperature
640 and soil moisture changes, Earth System Dynamics, 8, 477–493, https://doi.org/10.5194/esd-8-477-2017, 2017.

Mlawer, E. J., Taubman, S. J., Brown, P. D., Iacono, M. J., and Clough, S. A.: Radiative transfer for inhomogeneous atmospheres: RRTM, a validated correlated-k model for the longwave, Journal of Geophysical Research: Atmospheres, 102, 16 663–16 682, https://doi.org/10.1029/97JD00237, 1997.

Ngigi, S. N., Savenije, H. H. G., and Gichuki, F. N.: Land use changes and hydrological impacts related to up-scaling
645 of rainwater harvesting and management in upper Ewaso Ng'iro river basin, Kenya, Land Use Policy, 24, 129–140, https://doi.org/10.1016/j.landusepol.2005.10.002, 2007.

Nicholson, S.: The Turkana low-level jet: mean climatology and association with regional aridity, International Journal of Climatology, 36, 2598–2614, https://doi.org/10.1002/joc.4515, 2016a.

Nicholson, S. E.: Long-term variability of the East African 'short rains' and its links to large-scale factors, International Journal of Climatol-
650 ogy, 35, 3979–3990, https://doi.org/https://doi.org/10.1002/joc.4259, 2015.

Nicholson, S. E.: An analysis of recent rainfall conditions in eastern Africa, International Journal of Climatology, 36, 526–532, https://doi.org/10.1002/joc.4358, 2016b.

Nicholson, S. E.: Climate and climatic variability of rainfall over eastern Africa, Reviews of Geophysics, 55, 590–635, https://doi.org/10.1002/2016RG000544, 2017.

655 Niu, G.-Y., Yang, Z.-L., Mitchell, K. E., Chen, F., Ek, M. B., Barlage, M., Kumar, A., Manning, K., Niyogi, D., Rosero, E., Tewari, M., and Xia, Y.: The community Noah land surface model with multiparameterization options (Noah-MP): 1. Model description and evaluation with local-scale measurements, Journal of Geophysical Research: Atmospheres, 116, https://doi.org/10.1029/2010JD015139, 2011.

Otieno, G., Mutemi, J. N., Opijah, F. J., Ogallo, L. A., and Omondi, M. H.: The Sensitivity of Rainfall Characteristics to Cumulus Parameterization Schemes from a WRF Model. Part I: A Case Study Over East Africa During Wet Years, Pure and Applied Geophysics, https://doi.org/10.1007/s00024-019-02293-2, 2019.

Paegle, J. and Geisler, J. E.: The Effect of East African Topography on Flow Driven by Zonally Symmetric Forcing, Journal of the Atmospheric Sciences, 43, 1862–1872, https://doi.org/10.1175/1520-0469(1986)043<1862:TEOEAT>2.0.CO;2, 1986.

Parry, J.-E., Echeverria, D., Dekens, J., and Maitima, J.: Climate Risks, Vulnerability and Governance in Kenya: A review, p. 83, available at: https://www.iisd.org/pdf/2013/climate_risks_kenya.pdf, 2012.

Pleim, J. E.: A Combined Local and Nonlocal Closure Model for the Atmospheric Boundary Layer. Part I: Model Description and Testing, Journal of Applied Meteorology and Climatology, 46, 1383–1395, https://doi.org/10.1175/JAM2539.1, 2007.

Pohl, B. and Camberlin, P.: Intraseasonal and interannual zonal circulations over the Equatorial Indian Ocean, Theoretical and Applied Climatology, 104, 175–191, https://doi.org/10.1007/s00704-010-0336-1, 2011.

Pohl, B., Crétat, J., and Camberlin, P.: Testing WRF capability in simulating the atmospheric water cycle over Equatorial East Africa, Climate Dynamics, 37, 1357–1379, https://doi.org/10.1007/s00382-011-1024-2, 2011.

R Core Team: R: A Language and Environment for Statistical Computing, R Foundation for Statistical Computing, Vienna, Austria, https://www.R-project.org/, 2018.

Rauscher, S. A., Coppola, E., Piani, C., and Giorgi, F.: Resolution effects on regional climate model simulations of seasonal precipitation over Europe, Climate dynamics, 35, 685–711, 2010.

Rockel, B. and Geyer, B.: The performance of the regional climate model CLM in different climate regions, based on the example of precipitation, Meteorologische Zeitschrift, 17, 487–498, https://doi.org/10.1127/0941-2948/2008/0297, 2008.

Rummukainen, M.: State-of-the-art with regional climate models, WIREs Climate Change, 1, 82–96, https://doi.org/https://doi.org/10.1002/wcc.8, https://onlinelibrary.wiley.com/doi/abs/10.1002/wcc.8, 2010.

Russo, E., Kirchner, I., Pfahl, S., Schaap, M., and Cubasch, U.: Sensitivity studies with the regional climate model COSMO-CLM 5.0 over the CORDEX Central Asia Domain, Geoscientific Model Development, 12, 5229–5249, https://doi.org/10.5194/gmd-12-5229-2019, 2019.

Russo, E., Sørland, S. L., Kirchner, I., Schaap, M., Raible, C. C., and Cubasch, U.: Exploring the parameter space of the COSMO-CLM v5.0 regional climate model for the Central Asia CORDEX domain, Geoscientific Model Development, 13, 5779–5797, https://doi.org/10.5194/gmd-13-5779-2020, https://gmd.copernicus.org/articles/13/5779/2020/, 2020.

Saji, N., Goswami, B., Vinayachandran, P., and Yamagata, T.: A dipole mode in the tropical Indian Ocean, Nature, 401, 360–363, https://doi.org/https://doi.org/10.1038/43854, 1999.

Schmocker, J., Liniger, H. P., Ngeru, J. N., Brugnara, Y., Auchmann, R., and Brönnimann, S.: Trends in mean and extreme precipitation in the Mount Kenya region from observations and reanalyses, International Journal of Climatology, 36, 1500–1514, https://doi.org/10.1002/joc.4438, 2016.

Schulzweida, U.: CDO User Guide, https://doi.org/10.5281/zenodo.3539275, https://doi.org/10.5281/zenodo.3539275, 2019.

Skamarock, W. C., Klemp, J. B., Dudhia, J., Gill, D. O., Barker, D. M., Duda, M. G., yu Huang, X., Wang, W., and Powers, J. G.: A description of the Advanced Research WRF Version 3, NCAR Technical Note NCAR/TN-475+STR, https://doi.org/10.5065/D68S4MVH, 2008.

Slingo, J., Spencer, H., Hoskins, B., Berrisford, P., and Black, E.: The meteorology of the Western Indian Ocean, and the influence of the East African Highlands, Philosophical Transactions of the Royal Society of London A: Mathematical, Physical and Engineering Sciences, 363, 25–42, https://doi.org/10.1098/rsta.2004.1473, 2005.

695 Stratton, R. A., Senior, C. A., Vosper, S. B., Folwell, S. S., Boutle, I. A., Earnshaw, P. D., Kendon, E., Lock, A. P., Malcolm, A., Manners, J., Morcrette, C. J., Short, C., Stirling, A. J., Taylor, C. M., Tucker, S., Webster, S., and Wilkinson, J. M.: A Pan-African Convection-Permitting Regional Climate Simulation with the Met Office Unified Model: CP4-Africa, Journal of Climate, 31, 3485–3508, https://doi.org/10.1175/JCLI-D-17-0503.1, 2018.

Subin, Z. M., Riley, W. J., and Mironov, D.: An improved lake model for climate simulations: Model structure, evaluation, and sensitivity
700 analyses in CESM1, Journal of Advances in Modeling Earth Systems, 4, https://doi.org/10.1029/2011MS000072, 2012.

Sun, X., Xie, L., Semazzi, F., and Liu, B.: Effect of Lake Surface Temperature on the Spatial Distribution and Intensity of the Precipitation over the Lake Victoria Basin, Monthly Weather Review, 143, 1179–1192, https://doi.org/10.1175/MWR-D-14-00049.1, 2014.

Takle, E. S., Roads, J., Rockel, B., Gutowski, W. J., J., Arritt, R. W., Meinke, I., Jones, C. G., and Zadra, A.: Transferability Intercomparison: An Opportunity for New Insight on the Global Water Cycle and Energy Budget, Bulletin of the American Meteorological Society, 88,
705 375–384, https://doi.org/10.1175/BAMS-88-3-375, 2007.

Thiery, W., Davin, E. L., Panitz, H.-J., Demuzere, M., Lhermitte, S., and van Lipzig, N.: The Impact of the African Great Lakes on the Regional Climate, Journal of Climate, 28, 4061–4085, https://doi.org/10.1175/JCLI-D-14-00565.1, 2015.

Trewartha, G. T.: The Earth's problem climates, University of Wisconsin Press, 1981.

Ummenhofer, C. C., Gupta, A. S., England, M. H., and Reason, C. J. C.: Contributions of Indian Ocean Sea Surface Temperatures to
710 Enhanced East African Rainfall, Journal of Climate, 22, 993 – 1013, https://doi.org/10.1175/2008JCLI2493.1, 2009.

Velasquez, P., Messmer, M., and Raible, C. C.: A new bias-correction method for precipitation over complex terrain suitable for different climate states: a case study using WRF (version 3.8.1), Geoscientific Model Development, 13, 5007–5027, https://doi.org/10.5194/gmd-13-5007-2020, 2020.

Vergara-Temprado, J., Ban, N., Panosetti, D., Schlemmer, L., and Schär, C.: Climate Models Permit Convection at Much Coarser Resolu-
715 tions Than Previously Considered, Journal of Climate, 33, 1915–1933, https://doi.org/10.1175/JCLI-D-19-0286.1, publisher: American Meteorological Society Section: Journal of Climate, 2020.

Wainwright, C. M., Marsham, J. H., Keane, R. J., Rowell, D. P., Finney, D. L., Black, E., and Allan, R. P.: 'Eastern African Paradox'rainfall decline due to shorter not less intense Long Rains, npj Climate and Atmospheric Science, 2, 1–9, https://doi.org/https://doi.org/10.1038/s41612-019-0091-7, 2019.

720 Wiesmann, U., Gichuki, F. N., Kiteme, B. P., and Liniger, H.: Mitigating Conflicts Over Scarce Water Resources in the Highland-Lowland System of Mount Kenya, Mountain Research and Development, 20, 10–15, https://doi.org/10.1659/0276-4741(2000)020[0010:MCOSWR]2.0.CO;2, 2000.

Williams, A. P. and Funk, C.: A westward extension of the warm pool leads to a westward extension of the Walker circulation, drying eastern Africa, Climate Dynamics, 37, 2417–2435, https://doi.org/10.1007/s00382-010-0984-y, 2011.

725 Williams, K., Chamberlain, J., Buontempo, C., and Bain, C.: Regional climate model performance in the Lake Victoria basin, Climate Dynamics, 44, 1699–1713, https://doi.org/10.1007/s00382-014-2201-x, 2015.

Woodhams, B. J., Birch, C. E., Marsham, J. H., Bain, C. L., Roberts, N. M., and Boyd, D. F. A.: What Is the Added Value of a Convection-Permitting Model for Forecasting Extreme Rainfall over Tropical East Africa?, Monthly Weather Review, 146, 2757–2780, https://doi.org/10.1175/MWR-D-17-0396.1, 2018.

730 Woodhams, B. J., Birch, C. E., Marsham, J. H., Lane, T. P., Bain, C. L., and Webster, S.: Identifying Key Controls on Storm Formation over the Lake Victoria Basin, Monthly Weather Review, 147, 3365–3390, https://doi.org/10.1175/MWR-D-19-0069.1, 2019.

Wu, M., Nikulin, G., Kjellström, E., Belušić, D., Jones, C., and Lindstedt, D.: The impact of regional climate model formulation and resolution on simulated precipitation in Africa, Earth System Dynamics, 11, 377–394, https://doi.org/10.5194/esd-11-377-2020, 2020.

735   Yang, Z.-L., Niu, G.-Y., Mitchell, K. E., Chen, F., Ek, M. B., Barlage, M., Longuevergne, L., Manning, K., Niyogi, D., Tewari, M., and Xia, Y.: The community Noah land surface model with multiparameterization options (Noah-MP): 2. Evaluation over global river basins, Journal of Geophysical Research: Atmospheres, 116, https://doi.org/10.1029/2010JD015140, 2011.

Zamuriano, M., Froidevaux, P., Moreno, I., Vuille, M., and Brönnimann, S.: Synoptic and Mesoscale atmospheric features associated with an extreme Snowstorm over the Central Andes in August 2013, Natural Hazards and Earth System Sciences Discussions, 2019, 1–28, 2019.
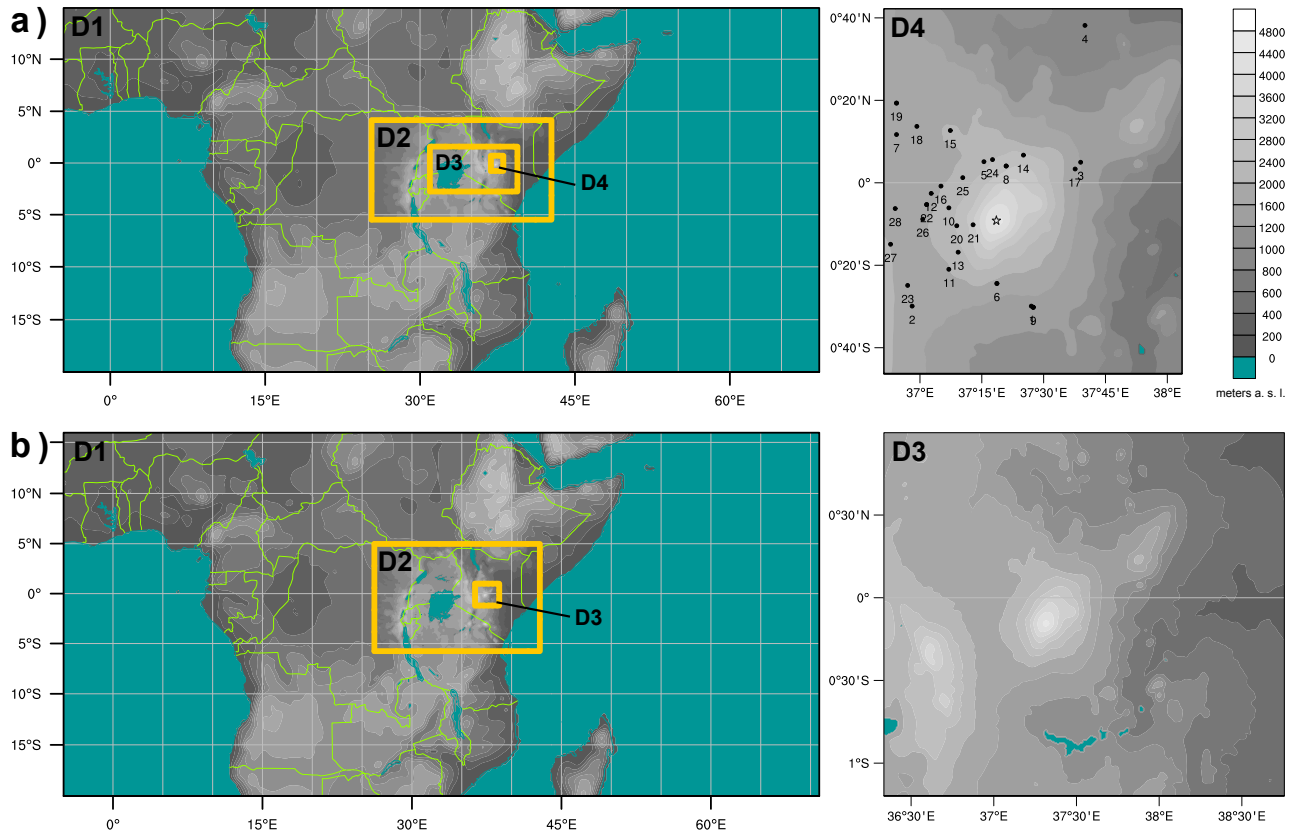
Figure 1. The two different nesting settings for the sensitivity experiments are depicted. The domains of the nesting ratio 1:3 are shown in row a) with the topography of the innermost nest D4 in the right panel. The domains of the nesting ratio 1:5 are shown in row b) with the topography of the innermost nest D3 in the right panel. D1 = 27/25 km, D2 = 9/5, D3 = 3/1, D4 = 1 km. The grey shading indicates elevation in meters above sea level using the WRF topography Global Multi-resolution Terrain Elevation Data (GMTED2010) provided by USGS. The location of the weather station data is provided in D04 and a more detailed description to each station is available in Table 2. The black star in D04 indicates the summit of Mount Kenya. Note that at least 30 grid points from the edge of the boundaries of an inner to an outer domain are used to avoid effects from the relaxation zone (spanning 5 grid points) between two nests (Rummukainen, 2010).
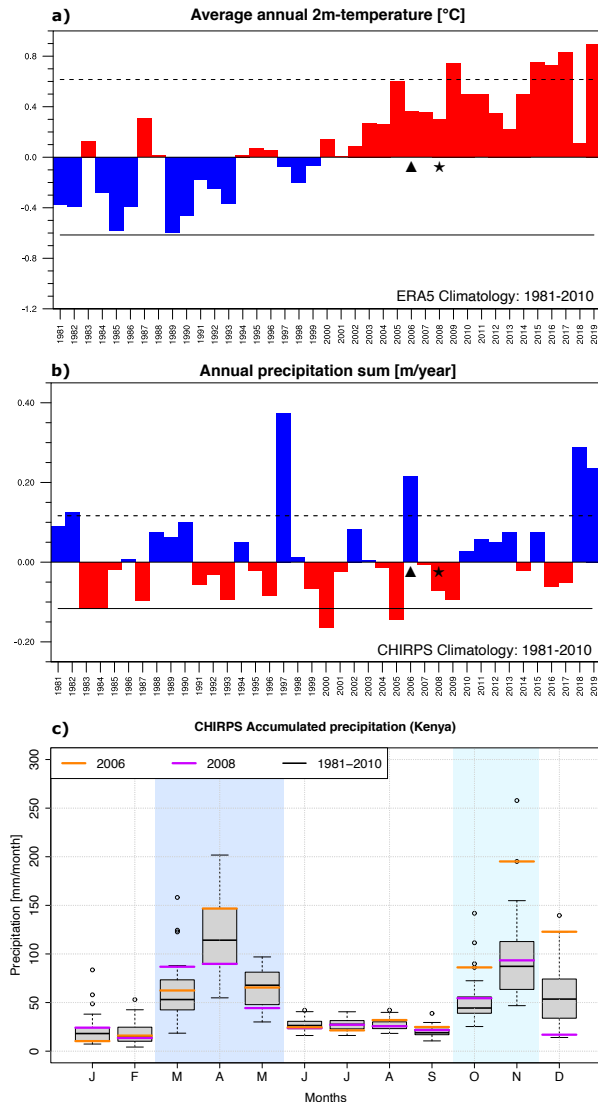
Figure 2. Annual anomalies of mean 2m-temperature (in °C) from ERA5 (Copernicus Climate Change Service (C3S), 2017) (a) and of precipitation (in m/year) from CHIRPS (Funk et al., 2015) (b). The anomalies are calculated with respect to the climatological mean of the years 1981 to 2010. The stippled (straight) lines illustrate plus (minus) one standard deviation. Monthly accumulated values of precipitation (in mm/month) for the selected year 2008 (in purple), and 2006 (in orange) compared to the climatology (1981-2010, in grey, using a Box-Whiskers plot) are shown in (c). All values are means over the territory of Kenya in each subplot. The whiskers extend to the value that is no more than 1.5 times the inter-quartile range away from the box. The values outside this range are defined as outliers and are plotted with dots. The dark and light blue shading indicates the 'long rains' and 'short rains', respectively.
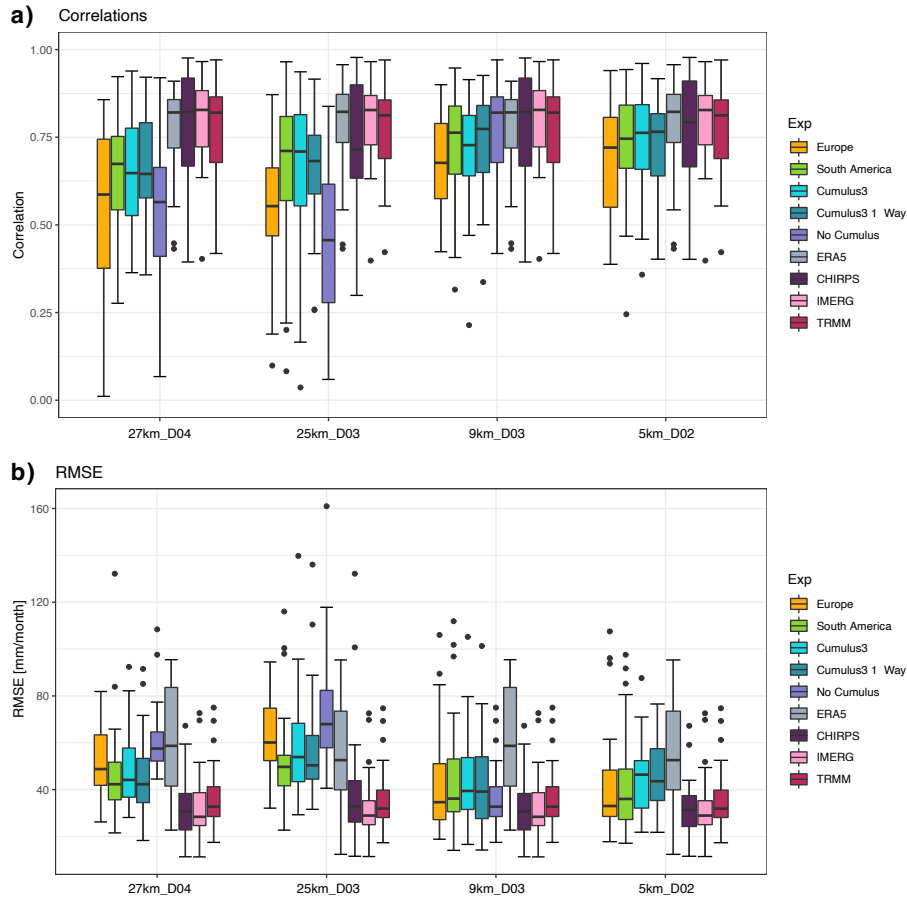
Figure 3. The temporal correlation (a) and root mean square error (RMSE) (b) between the annual cycle of year 2008 of measured and simulated monthly precipitation sums at the nearest grid point to the station's location are shown for the different parameterization options (see legend to the right, Table 1), grouped by the different nesting options and number of nests. The box and whisker plots show the values in relation to 28 stations for the different domains with 1 km spatial resolution. The whiskers extend to the value that is no more than 1.5 times the inter-quartile range away from the box. The values outside this range are defined as outliers and are plotted with dots.
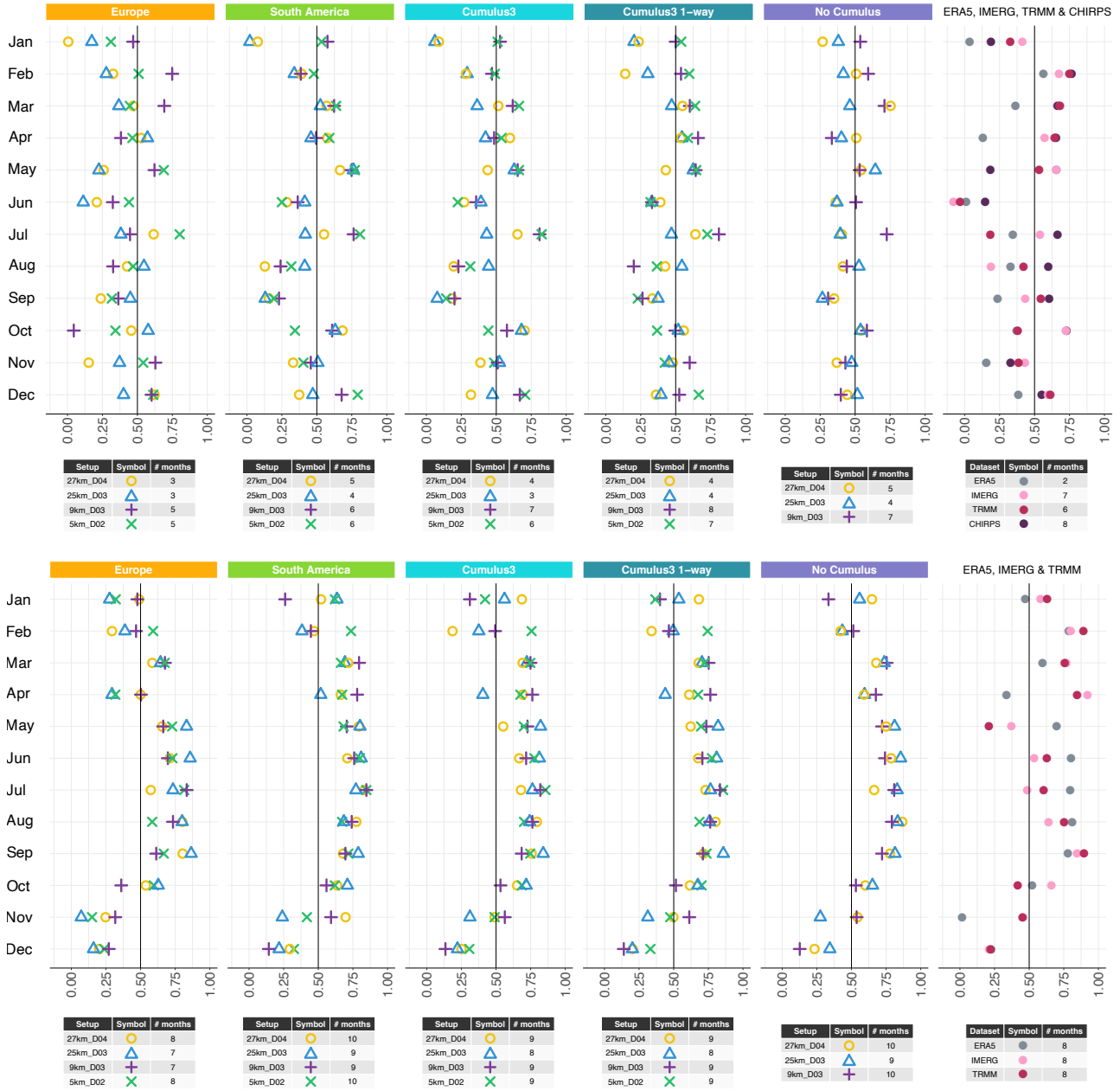
Figure 4. Pattern correlation of monthly precipitation sums of year 2008 between weather station data and the respective WRF simulation (upper row), and between CHIRPS and the respective WRF simulation (interpolated onto the CHIRPS grid, lower row). The different panels indicate the different parameterization options (Table 1), and the symbols stand for the different nesting options. The labelling of the symbols is given in the table below each panel, along with the number of months (# months) in which the nesting option obtain correlation patterns above the reference value of 0.50 (a moderate correlation used to visually evaluate the performance of nesting options). The last panel on each row represents the gridded data sets used throughout the paper. Even if the gridded data sets are interpolated onto different domains for each independent set-up, here only one setting is shown (27 km_D4). The rest was omitted as only marginal changes can be observed.
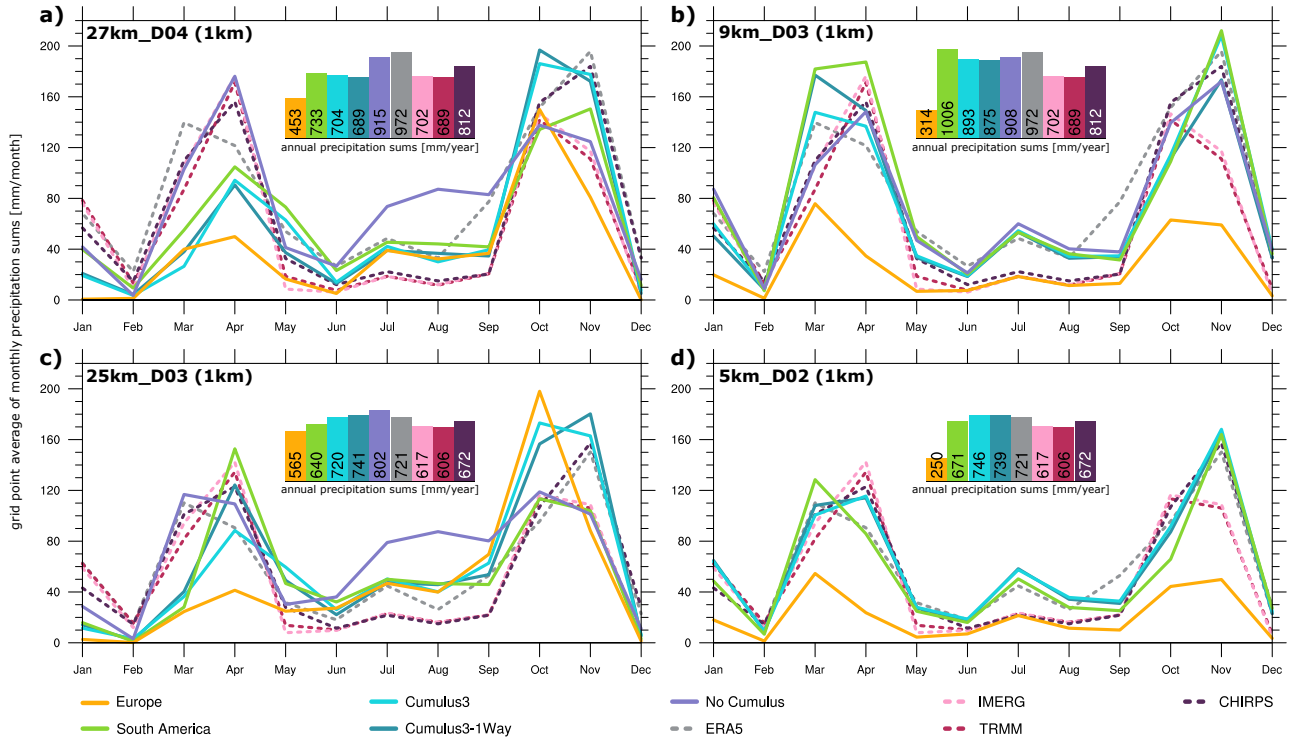
Figure 5. Grid point averages of monthly precipitation sums in mm/month of year 2008 of the innermost domain (1 km) for each of the tested set-ups: 27 km (a), 9 km (b), 25 km (c) and 5 km (d). The 5 tested parameterization options are included, along with the driving reanalysis ERA5 and the three observational gridded data sets (IMERG, TRMM and CHIRPS). All the gridded data sets are plotted with different shades of pink, while ERA5 is colored in grey. The inset of a bar plot in each panel indicates the grid point average annual precipitation sum in mm/year for each parameterization option and gridded data set.
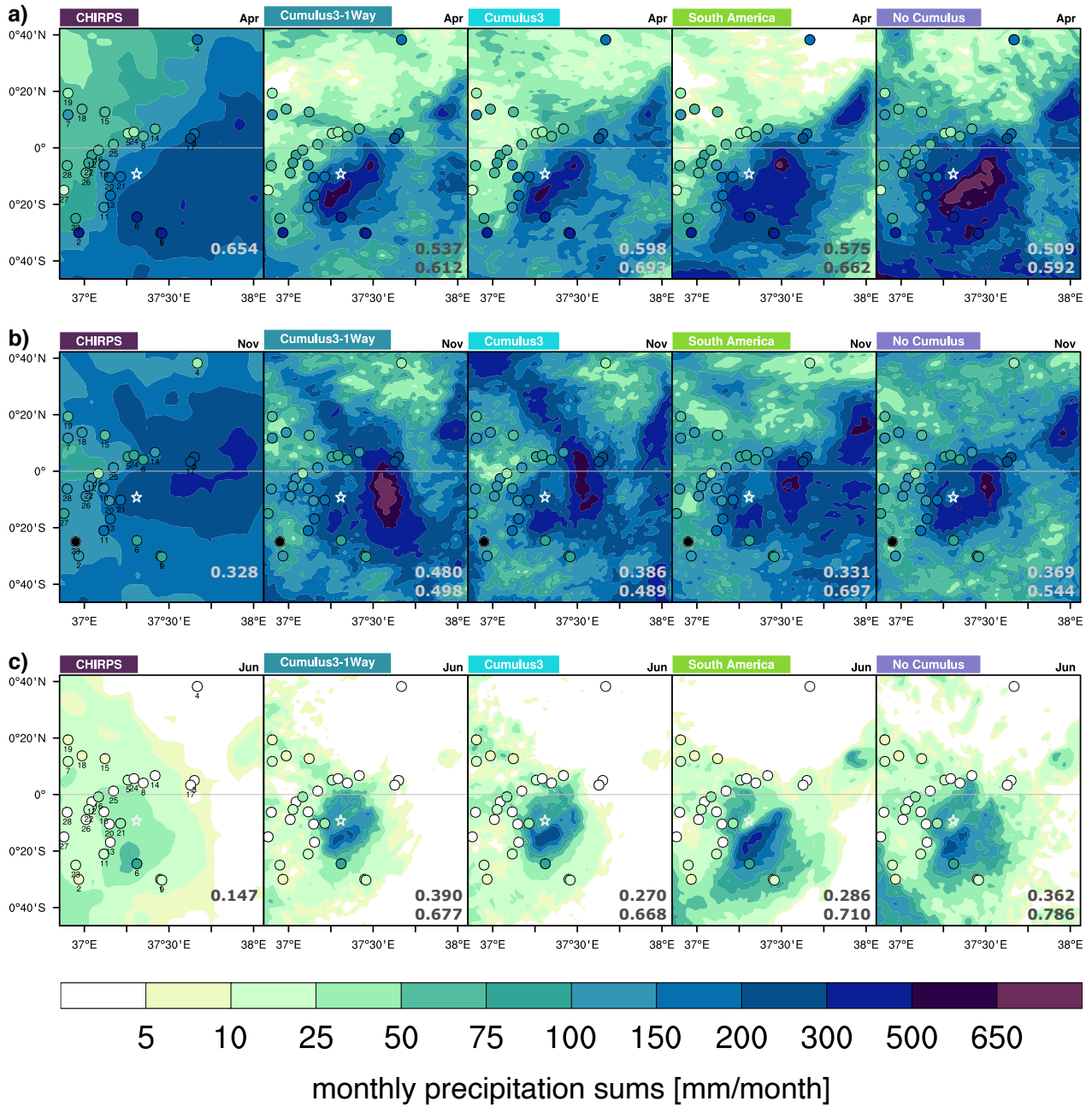
Figure 6. Monthly precipitation sums for a) April 2008 ('long rains'), b) November 2008 ('short rains') and c) June 2008 (dry season) in mm/month for the innermost domain (1 km) of the 4 nested domain setup, with the outermost domain of 27 km resolution and a nesting ratio 1:3 for the different parameterization setups (see Table 1). Weather station data are described in Table 2. The white star indicates the summit of Mount Kenya, and missing values are marked in black. The numbers in the lower right corner of each panel indicate the spatial correlation with respect to the stations (upper line) and CHIRPS (lower line).
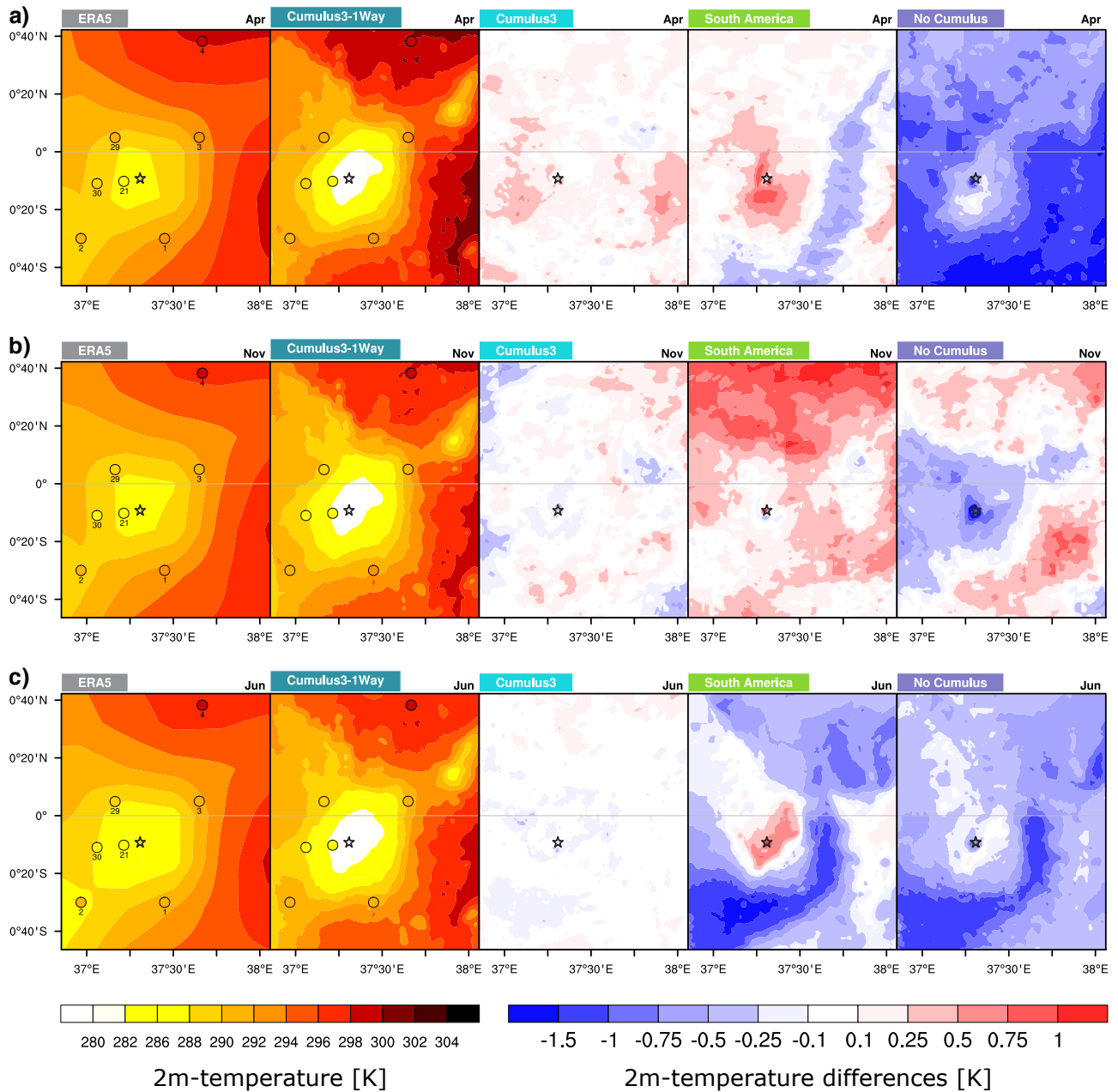
Figure 7. Monthly 2-metre temperature averages for a) April 2008 ('long rains'), b) November 2008 ('short rains') and c) June 2008 (dry season) in K are shown for the innermost domain (1 km) of the 4 nested domain setup, with the outermost domain of 27 km resolution and a nesting ratio 1:3 for the different parameterization setups (Table 1). Absolute values are given for ERA5 and the "Cumulus3 1-way" option. The others depict differences compared to the "Cumulus3 1-way" option. Weather station data are described in Table 2. The black star indicates the summit of Mount Kenya.

Table 1. Experimental design of the sensitivity simulations: Name of the experiment, parameterizations used and other parameters important for each experiment such as nesting option and ratio, number of domains, the spatial resolution of the used domains and their corresponding names as they appear in Fig. 1. Domains written in bold indicate that the according cumulus parameterization is turned on, while domains printed in normal fonts do not parameterize cumulus processes. The last column provides the name of the innermost domain, used in Figures to identify nesting and resolution options. All other options used for the simulation can be found in the namelist files on Zenodo (see Code and data availability section).

| Name | Parameterizations | | | Other parameters | | | | | Name |
	Cumulus	LW-Rad.	PBL	Nesting	Nest ratio	# dom	Resolutions	doms in Fig. 1	1km domain
Europe	Grell-Freitas	CAM	ACM2[1]	2-way	1:3	4	27, 9, 3, 1 km	(a) **D1**, **D2**, D3, D4	27km_D04
	Grell-Freitas	CAM	ACM2	2-way	1:3	3	9, 3, 1 km	(a) **D2**, D3, D4	9km_D03
	Grell-Freitas	CAM	ACM2	2-way	1:5	3	25, 5, 1 km	(b) **D1**, D2, D3	25km_D03
	-	CAM	ACM2	2-way	1:5	2	5, 1 km	(b) D2, D3	5km_D02
South America	Kain-Fritsch	RRTM[2]	YSU[3]	2-way	1:3	4	27, 9, 3, 1 km	(a) **D1**, **D2**, D3, D4	27km_D04
	Kain-Fritsch	RRTM	YSU	2-way	1:3	3	9, 3, 1 km	(a) **D2**, D3, D4	9km_D03
	Kain-Fritsch	RRTM	YSU	2-way	1:5	3	25, 5, 1 km	(b) **D1**, D2, D3	25km_D03
	-	RRTM	YSU	2-way	1:5	2	5, 1 km	(b) D2, D3	5km_D02
Cumulus3	Grell-Freitas	RRTM	YSU	2-way	1:3	4	27, 9, 3, 1 km	(a) **D1**, **D2**, D3, D4	27km_D04
	Grell-Freitas	RRTM	YSU	2-way	1:3	3	9, 3, 1 km	(a) **D2**, D3, D4	9km_D03
	Grell-Freitas	RRTM	YSU	2-way	1:5	3	25, 5, 1 km	(b) **D1**, D2, D3	25km_D03
	-	RRTM	YSU	2-way	1:5	2	5, 1 km	(b) D2, D3	5km_D02
Cumulus3 1-way	Grell-Freitas	RRTM	YSU	1-way	1:3	4	27, 9, 3, 1 km	(a) **D1**, **D2**, D3, D4	27km_D04
	Grell-Freitas	RRTM	YSU	1-way	1:3	3	9, 3, 1 km	(a) **D2**, D3, D4	9km_D03
	Grell-Freitas	RRTM	YSU	1-way	1:5	3	25, 5, 1 km	(b) **D1**, D2, D3	25km_D03
	-	RRTM	YSU	1-way	1:5	2	5, 1 km	(b) D2, D3	5km_D02
No Cumulus	-	RRTM	YSU	1-way	1:3	4	27, 9, 3, 1 km	(a) D1, D2, D3, D4	27km_D04
	-	RRTM	YSU	1-way	1:3	3	9, 3, 1 km	(a) D2, D3, D4	9km_D03
	-	RRTM	YSU	1-way	1:5	3	25, 5, 1 km	(b) D1, D2, D3	25km_D03
	-	RRTM	YSU	1-way	1:5	2	5, 1 km	(b) D2, D3	5km_D02[4]

[1] Asymmetric Convection Model Version2

[2] Rapid Radiative Transfer Model

[3] Yonsei University

[4] This simulation is identical to the last one in "Cumulus3 1-way" and therefore it is only shown related to the "Cumulus3 1-way" parameterization option in Fig. 3 and 4

Table 2. Weather station information: Station number used in our study (labels in Figs. 1, 6 and 7), station name, location (latitude and longitude), altitude (in meters above sea level), number of missing values, variables available and station ID from WMO (first three lines) or from Table 1 in Schmocker et al. (2016). RR stands for precipitation and T2 for 2-metre temperature.

Number	Station	Lat	Lon	Altitude [m]	# missing	variable	ID
1	Embu WMO	-0.5	37.45	1493	0	RR, T2	637200
2	Nyeri WMO	-0.5	36.967	1759	0	RR, T2	637170
3	Meru WMO	0.083	37.65	1554	0	RR, T2	636950
4	Archers Post	0.6375	37.6675	839	0	RR, T2	1
5	Ardencaple Farm	0.0852	37.258	2271	0	RR	2
6	Castle Forest Station	-0.4083	37.3107	1927	0	RR	5
7	El Karama	0.1952	36.9038	1781	0	RR	95
8	Embori Farm	0.0677	37.3482	2691	0	RR	12
9	Embu Met Station	-0.5047	37.4579	1743	0	RR	14
10	Gathiuru Forest Station	-0.1018	37.1159	2333	0	RR	17
11	Hombe Forest Station	-0.3508	37.1158	2017	0	RR	20
12	Jacobson Farm	-0.0432	37.0444	1913	0	RR	23
13	Kabaru Forest Station	-0.2814	37.1535	2279	0	RR	25
14	Kisima Farm	0.1118	37.4181	2465	0	RR	35
15	Loldaiga Farm	0.2117	37.1219	2135	0	RR	34
16	Loruku Farm	-0.0136	37.0839	1896	0	RR	38
17	Meru Forest Station	0.0557	37.6277	1737	0	RR	45
18	Mogwoni Ranch	0.2284	36.9862	1683	0	RR	47
19	Mpala Farm	0.3227	36.9038	1844	0	RR	48
20	Naro Moru Gate Station	-0.1744	37.148	2471	0	RR	61
21	Naro Moru Met Station	-0.1704	37.214	3048	0	RR, T2	62
22	Nicholson Farm	-0.0886	37.0259	1916	0	RR	66
23	Nyeri Mow	-0.4162	36.9489	1854	92	RR	67
24	Ol Donyo Farm	0.0938	37.2929	2375	0	RR	69
25	Ontulili Forest Station	0.0206	37.1723	2056	0	RR	75
26	Satima Farm	-0.1475	37.0101	1944	0	RR	82
27	Solio Ranch	-0.2493	36.8797	1943	0	RR	87
28	Tharua Farm	-0.1046	36.8985	1865	0	RR	92
29	Kalalu	0.0817	37.1638	2027	0	T2	-
30	Munyaka	-0.1833	37.0596	2048	0	T2	-